DEVELOPMENT OF KINETOSTATIC DESIGN METHODOLOGY FOR AIRPLANE FLAP MECHANISMS

A Thesis Submitted to
the Graduate School of Engineering and Sciences of
İzmir Institute of Technology
in Partial Fulfillment of Requirements for the Degree of

MASTER OF SCIENCE

in Mechanical Engineering

by
Gökhan ARSLAN

December 2022
İZMİR

ACKNOWLEDGEMENTS

I would like to express my deepest appreciation to my advisor Prof. Dr. Gökhan Kiper for his endless support at any time.

I am also extremely grateful to Dr. Lütfi Ertong and Abdi Orhan Yavuz for their great assistance from TUSAŞ.

Besides, I am deeply indebted to my family for their continuous support.

This thesis was funded by The Scientific and Technological Research Council of Turkey (TÜBİTAK) 2210-D program, I am extremely grateful to them, as well.

ABSTRACT

DEVELOPMENT OF KINETOSTATIC DESIGN METHODOLOGY FOR AIRPLANE FLAP MECHANISMS

The problem focused on this thesis is to minimize the fairing drag of dropped-hinge trailing edge flap mechanism of an aircraft. The background knowledge and literature review about the trailing edge flaps and mechanisms are presented, and two patents are examined. Accordingly, a parametric model for a double circular slotted arc track mechanism with a screw jack drive for a trailing edge flap is presented. This model is used in the kinetostatic design methodology. The methodology is applied for a small aircraft as a case study. The main novelty of this thesis is these model and methodology. According to the results, motor torque requirement for the screw jack is determined. The fairing depth is considerably reduced compared to a dropped hinge type mechanism.

Keywords: *Fairing Size, Trailing Edge Flaps, High Lift Devices, Circular Arc Track Mechanism, Remote Center of Motion*

ÖZET

UÇAK FLAP MEKANİZMALARI İÇİN KİNETOSTATİK TASARIM YÖNTEMİ GELİŞTİRİLMESİ

Bu tezde odaklanılan problem bir uçağın düşük menteşe firar kenarı kanatçık mekanizma karenajının yarattığı sürüklenme kuvvetini en aza indirmektir. Firar kenarı kanatçıkları ve mekanizmaları hakkında bilgi altyapısı oluşturularak, literatür taranmış ve iki patent incelenmiştir. Bir firar kenarı kanatçık için kriko vida tahrikli çift raylı çembersel yay mekanizması parametrik modeli sunulmuştur. Bu model, geliştirilen kinetostatik tasarım yönteminde kullanılmıştır. Bu yöntem, küçük bir uçak için örnek çalışma olarak uygulanmıştır. Bu tezin özgün kısmı bu model ve yöntemdir. Sonuçlara göre kriko vidası için gerekli motor tork ihtiyacı belirlenmiştir. Kanatçığın doğrudan mesnetlendiği duruma göre karenaj derinliği önemli ölçüde azaltılmıştır.

Anahtar Kelimeler: *Karenaj Boyutu, Firar Kenarı Kanatçıkları, Yüksek Kaldıraç Tertibatı, Raylı Çembersel Yay Mekanizması, Uzak Hareket Merkezi*

TABLE OF CONTENTS

LIST OF FIGURES

Figure **Page**

Figure **Page**

LIST OF TABLES

CHAPTER 1

INTRODUCTION

An aircraft's mission profile basically consists of take-off, cruise and landing phases. The time of flight being covered by an aircraft is mostly during the cruise phase. Therefore, it is a common practice to optimize the wings for the cruise flight efficiency which helps to decrease operational costs (Jie, 2009). However, this is generally not sufficient for a complete mission profile because aircrafts may demand higher lift values to be operable by the limits of runaway lengths during the take-off and landing phases. Thus, wings may be equipped with high lift devices (HLD), which provide additional lift and required L/D (lift/drag ratio) when they are deployed while keeping the cruise performance minimally deteriorated (Pires, 2007; Zaccai, 2014; Flaig & Hilbig, 1993). These HLDs can be leading-edge slats and leading- or trailing-edge flaps.

Before getting into the flap details, airfoil nomenclature is presented according to Fig. 1. In Fig. 1 the leading and trailing edges are connected by the chord line. When a line set between upper and lower surfaces of the airfoil is drawn perpendicular to chord line, airfoil thickness values are obtained and the mean camber line is obtained by connecting the midpoints. Camber is the maximum distance between chord and mean camber lines (Anderson, 2010).

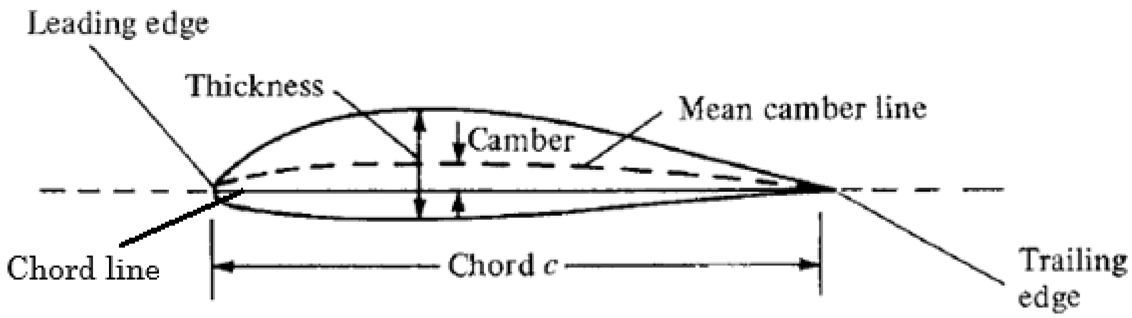

Figure 1. Nomenclature for an airfoil (Source: Anderson, 2010)

The flaps provide that additional lift by transiently changing the wing airfoil geometry (McCormick, 1979). They can be classified as powered and unpowered flaps. The powered ones are referred to jet flaps which provide the jet flux from the trailing edge, in the form of air sheets at an angle to the freestream (McCormick, 1979; Williams et al., 1961). Although HLD equipped with such systems are able to increase the maximum value of lift coefficient ($C_{L,max}$) up to 7, they increase the system complexity as well (Bertin & Cummings, 2014). On the contrary, the unpowered ones are referred to mechanical flaps (Fig. 2).

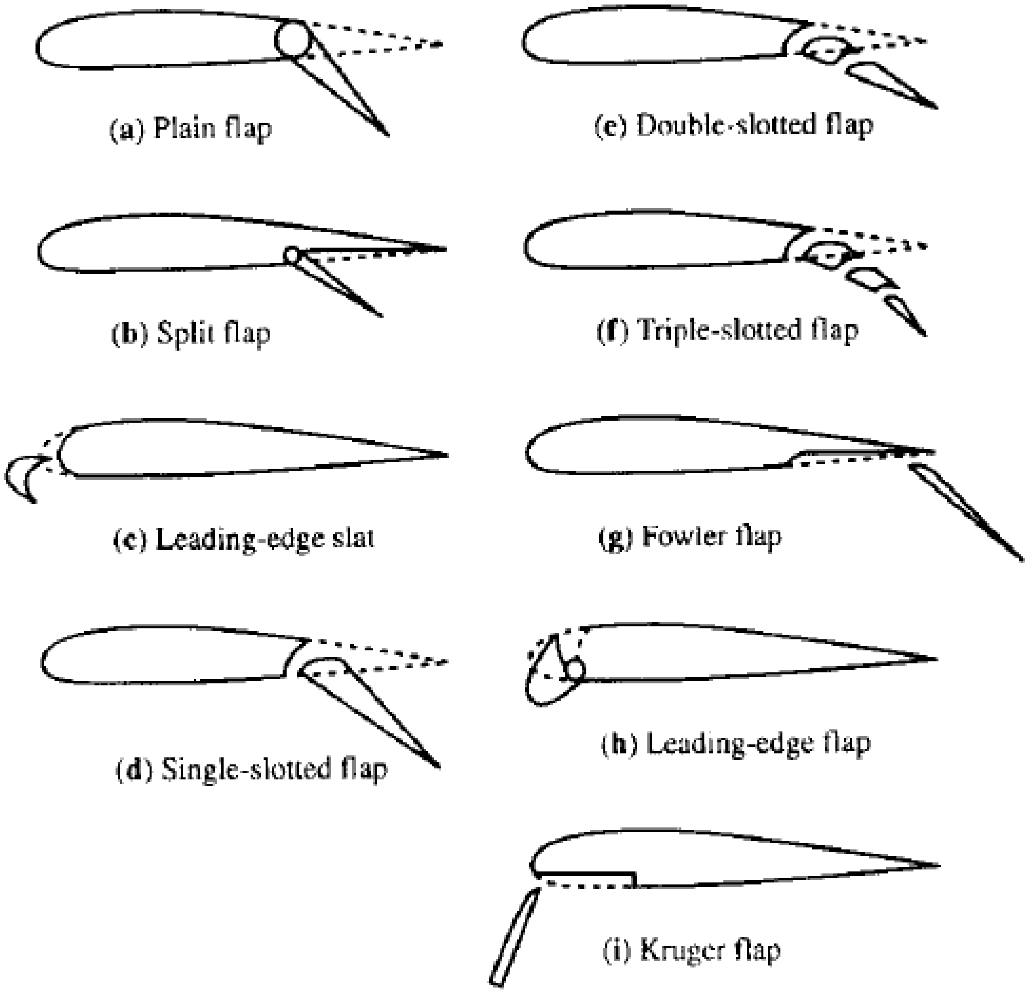

Figure 2. Several types of HLD (Source: Anderson, 1999)

Typically, plain airfoils have $C_{L,max}$ values around 1.4 (Anderson, 1999). The focus in this thesis is on trailing edge flaps, therefore only the trailing edge flaps shown in Fig. 2 are examined below.

The plain flap shown in Fig. 2(a) has a hinged part at its rear section, allowing the flap to be rotated downwards. This rotation increases the effective camber of the airfoil which results in increased lift, drag and pitch moment (Anderson, 1999). Also, flow separation may develop after 20° of flap deployment, which is a limiting factor (Pires, 2007).

The split flap shown in Fig. 2(b) has a hinged part on the bottom surface of its rear section, allowing the flap to be rotated downwards, similar to the case Fig. 2(a). Although the effective camber is increased again, more drag is developed compared to the plain flap. This was invented in 1920 and their use is not common in modern airplanes due to their drag values (Anderson, 1999).

The single-slotted flap shown in Fig. 2(d) allows the flow to pass through the gap between top and bottom surfaces (Anderson, 1999). The high-pressure air flows through that slot while re-energizing and stabilizing the boundary layer. The flow separation is delayed while 35° of flap deflection is achievable, in such a way. Besides, it increases the wing area slightly when it is deployed, which enhances the lift not much (Pires, 2007).

The double-slotted flap shown in Fig. 2(e) allows the flow to pass through two slots while allowing larger flap deployments (Anderson, 1999; Pires, 2007). Although this configuration enhances the lift slightly, it increases mechanical complexity (Anderson, 1999).

The triple-slotted flap shown in Fig. 2(f), similarly, allows the flow to pass through three slots while allowing flap deflections about 80°. Also, their mechanical complexity is much higher than the less slotted flaps (Pires, 2007). Such a flap is encountered on aircrafts with high wing loadings, such as Boeing 747 (Anderson, 1999).

The Fowler flap shown in Fig. 2(g) experiences Fowler motion which increases effective camber and wing area since it both rotates and translates. The slotted flaps (single-, double- and triple-) may be combined with this Fowler flap concept, which is the case for Boeing 747' triple-slotted flaps, as an instance (Anderson, 1999; Pires, 2007).

The approximate $C_{L,max}$ values of typical airfoils equipped with some of these trailing edge flaps are given in Table 1, in order to emphasize their contribution to lift.

The common actuation types for these flaps are dropped-hinge (simple hinge), four-bar, link-track and hooked-track mechanisms. Typically, the actuation can be provided via linear or rotary actuators for dropped-hinge and four-bar mechanisms. Besides, rotary and linear actuators are used for link-track and hooked-track mechanisms, respectively (Lima et al., 2021; Zaccai et al., 2016). Although it is not that common, circular arc track mechanisms were applied to Boeing 707-320 trailing-edge flap mechanisms, in early 1960's as well (Rudolph, 1996).

Table 1. Coefficient of lift values for typical airfoils equipped with several types of trailing edge flaps (Source: Anderson, 1999)

FLAP TYPE	$C_{L,max}$
Plain Flap	2.4
Split Flap	2.6
Single-slotted Flap	2.9
Double-slotted Flap	3

In this thesis, the parametric model of a double circular slotted arc track mechanism with a screw jack drive for a single-slotted trailing-edge flap is developed. The origin of the problem is to reduce fairing size of the dropped-hinge trailing-edge flap mechanism in order to reduce fairing drag. The model includes kinematics, static and dynamic (if necessary) force analyses of the said mechanism. Accordingly, required motor torque calculations are performed. Then, a design methodology is presented for this model. Furthermore, a methodology is illustrated with a case study.

CHAPTER 2

LITERATURE REVIEW

In this Chapter, related studies, two patents and current trailing-edge flap mechanisms are reviewed under three sections to gain insight and develop background knowledge about the topic.

2.1. Academic Research

Pires (2007) introduced a design methodology for trailing edge HLD including synthesis and optimization of aeronautical mechanisms using SYNAMEC module, which is a European Union project for type synthesis of mechanisms and their design, preliminary sizing methods, weight and cost estimations, reliability and maintainability assessments with a case study demonstration.

Jie (2009) implemented a swing-arm mechanism to the trailing edge flaps of an aircraft (Flying crane project). The work achieved competitive results in the reduction of fairing size problem for mechanism stowage and included fairing size comparison of his/her work with several types of existing mechanisms. Also, driving motor power calculations and mass estimation were presented.

Zaccai et al. (2016) developed a design methodology for dropped-hinge, four-bar, link-track and hooked-track trailing edge flap mechanisms. In the first stages, attachment points between mechanism and flap were determined by considering 3-D flap kinematics. Then, the synthesis of the four mechanisms were implemented. After that, mechanism links and transmission sizing procedure were given. In the last stages, the weight estimation of VFW-614 hooked-track mechanism and a comparative study for flap actuation mechanism of Boeing 777 were covered in two case studies.

Shi et al. (2019) introduced a direct design method for HLD design framework. Firstly, parametric models for dropped-hinge and link-track mechanisms were developed with their constraints. Then, computational fluid dynamics (CFD) tools were utilized to validate whether the solver was applicable or not and a surrogate model was created.

Later, the weighted functions accounting for aerodynamics, weight and cost were determined and optimized using genetic algorithm. The optimized mechanism values for the two types of mechanisms were presented.

2.2. Patents

According to the patent illustrated in Fig. 3, the actuation is provided via two independent actuators; a translational driver actuator housed at rear portion of the wing and a rotary actuator housed in trailing edge flap itself. Since the actuators are independent, various configurations for the flap are allowable. It may be advantageous to configure electro-hydraulic actuator (EHA) for rotary actuator, so that controlling will be easier and torque level is appropriate. Besides, the axis of rotation for the rotary actuator may be located between 30 to 40 percent of flap chord to actuate the flap with less excessive torque by considering the aerodynamic forces/moments. Additionally, this design does not require any fairings. Besides, the flaps may be used as air brakes in this design (Guering, 2015).

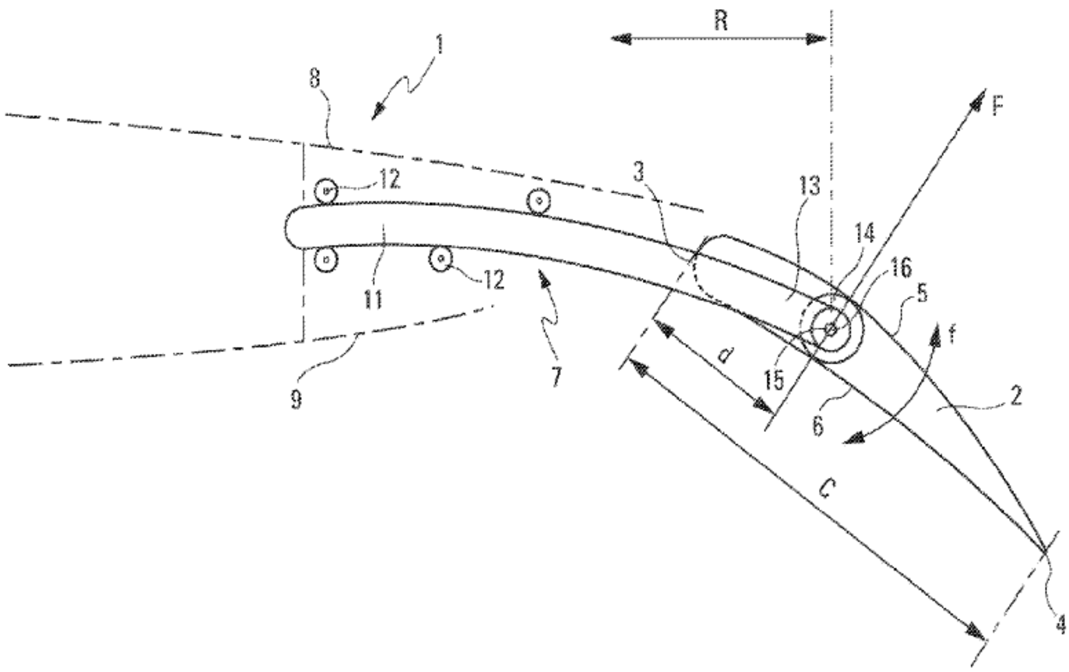

Figure 3. Side view of HLD at a deployed configuration (Source: Guering, 2015)

According to the patent illustrated in Fig. 4, rib 4 may preferably be connected to rear spar 16 via bolts or rivets (not shown). The circular track inside the rib 4 may preferably be constant radius of curvature. The rollers are guided inside the track throughout the flap deployment. The actuation is provided via linear rod 13 which may be powered by a central driving unit with the necessary gearing for axial adjustments of motion. The element 45 is hinged to linear rod 13 to support the loads. The sliding carriage 14 is hinged to the part housing the rollers. The guide 20 at the end of trailing end of the linear rod 19 may not be included in design since trailing end of linear rod 19 is able to rotate freely upward/downward with respect to rib 4, throughout the flap deployment. Proper fairing design is required to protect the actuating mechanism and to have better aerodynamics. It is not noted that flushing of rib 4 smoothly over the upper surface deteriorate the aerodynamic performance (Vervliet et al., 2018).

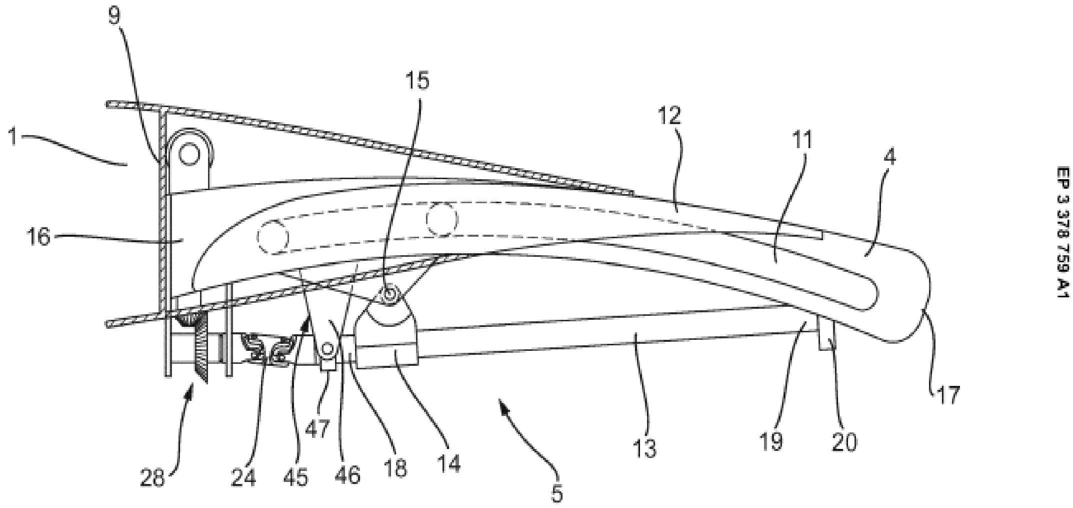

Figure 4. Side view of the HLD with actuation system in cruise (retracted) configuration (Source: Vervliet et al., 2018)

2.3. Current (Exemplary) Trailing Edge Flap Mechanisms

Dropped-hinge mechanism of DC-10/MD-11 aircrafts operate double-slotted trailing edge flaps (articulating vane/main type). Since the rotation is about the axis of revolute joint located at lowermost portion of the mechanism in Fig. 5, required fairing depth to house the mechanism is deep (Rudolph, 1996).

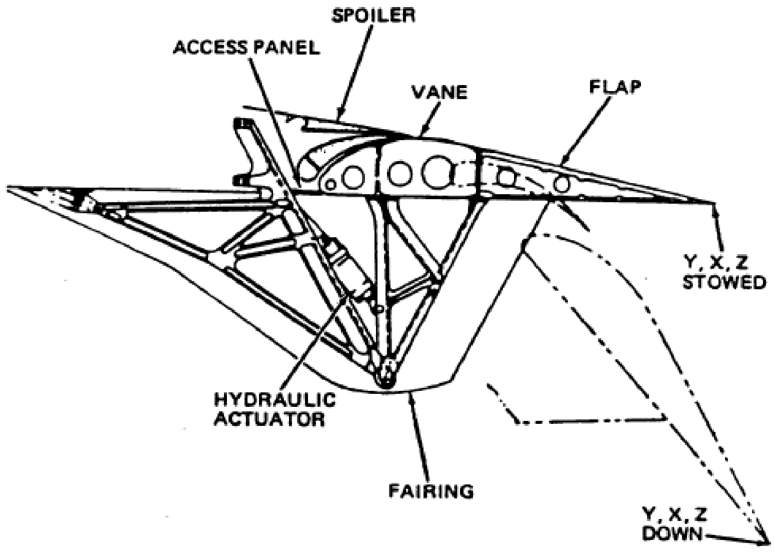

Figure 5. Dropped-hinge flap of DC-10/MD-11 for two configurations of flap (Source: Rudolph, 1996)

The single-slotted trailing edge flaps of Boeing 747SP are equipped with a four-bar linkage (upside-down type) as shown in Fig. 6, both inboard and outboard of the wing. This mechanism does not require fairings, which makes it lighter and less complex (Rudolph, 1996).

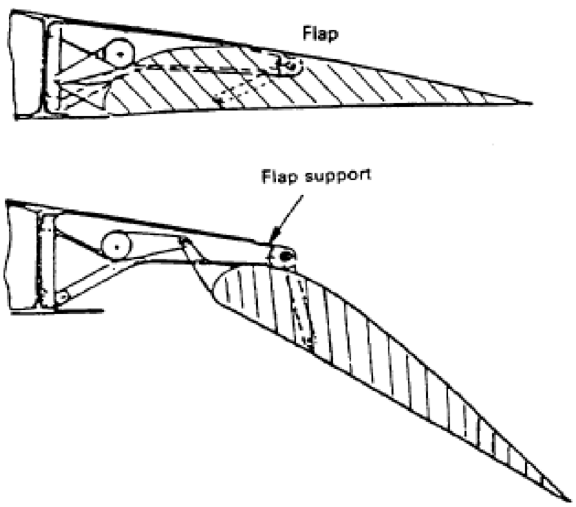

Figure 6. Upside-down four-bar mechanism of Boeing 747SP (Source: Rudolph, 1996)

The Boeing link-track mechanism in Fig. 7 can be applied to both single- and double-slotted flaps (vane/main type). Although such a mechanism requires fairings, its size is smaller and shallower than fairings of Airbus 320 and 330/340 link-track mechanisms (Rudolph, 1996).

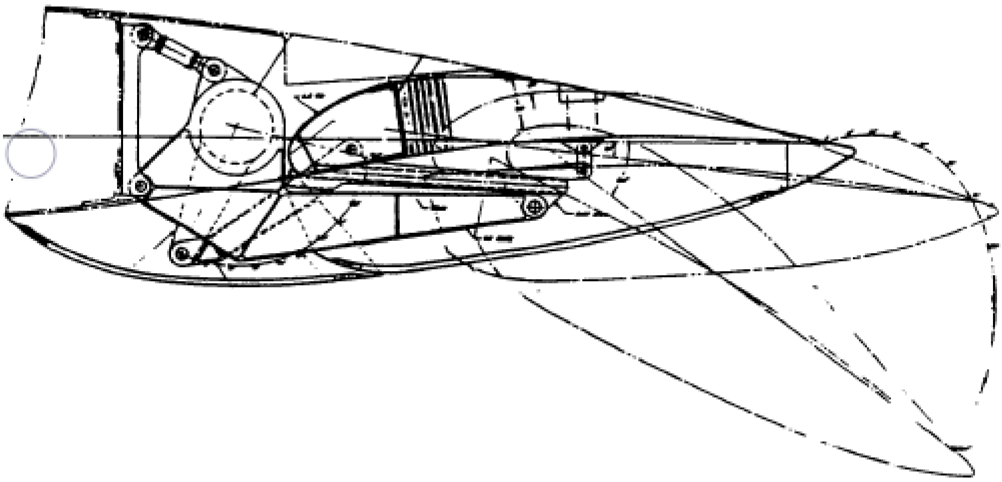

Figure 7. Link-track mechanism for single-slotted flap of Boeing for two configurations of flap (Source: Rudolph, 1996)

The Airbus 310 inboard double-slotted flap (articulating vane/main type) in Fig. 8 is operated by a hooked-track mechanism, which is actuated by screw jacks. The track inside is I-beam type, which guides cantilevered rollers. The fairing size is said to be moderate. As a side note, better wear characteristics can be achieved using links instead of rollers i.e., contact type being line or surface matters (Rudolph, 1996).

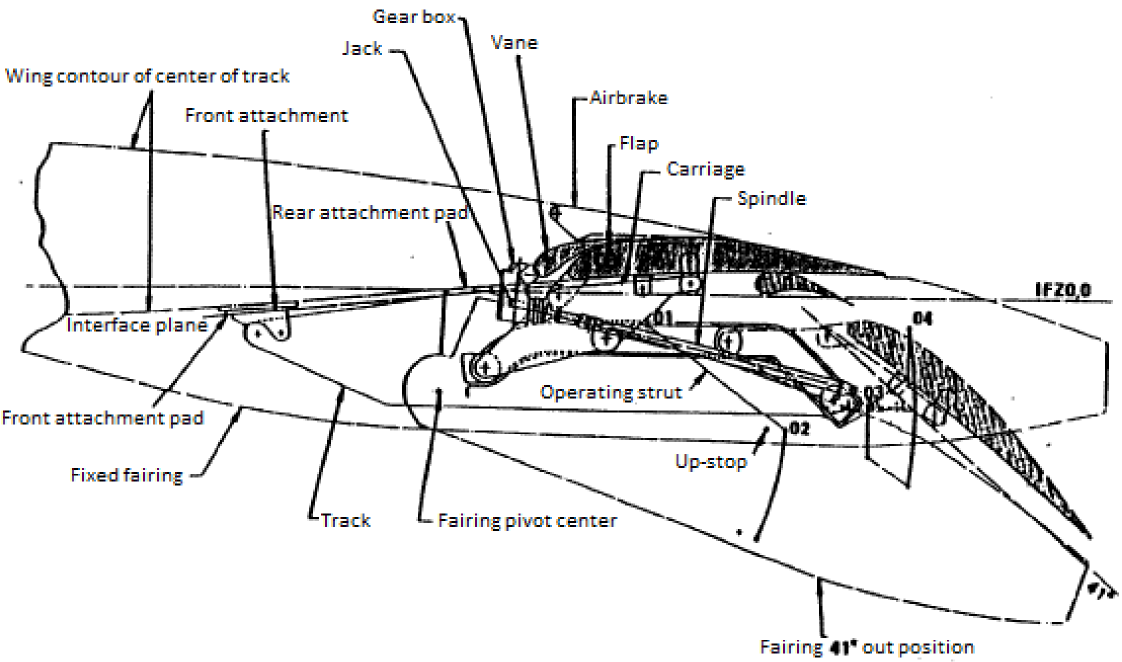

Figure 8. Hooked-track mechanism of Airbus 310 inboard trailing-edge flaps (Source: Rudolph, 1996)

The Fowler motion is limited for circular arc track mechanisms since the mechanism only rotates about a specified axis with a certain radius and does not translate additionally. Also, such mechanisms kinematically resemble dropped-hinge ones since both types rotate about a specific axis. Besides, such mechanisms may not require flap fairings, which is the case for Boeing 707-320, as shown in Fig. 9 (Rudolph, 1996).

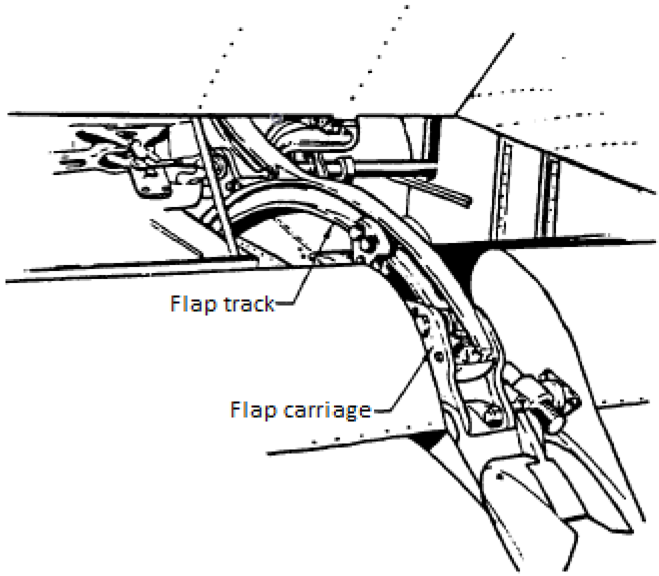

Figure 9. Circular arc track mechanism of Boeing 707-320 (Source: Rudolph, 1996)

CHAPTER 3

PARAMETRIC MODEL

In this Chapter, a parametric model of the circular arc track mechanism with a screw jack drive is developed. The design constraints are:

1) The flap size and the rotation axis of the flap are given (assumed as the origin for the model), thus, flap will only rotate, not translate.
2) Maximum amount of flap rotation from the retracted configuration is given.

3.1. Kinematic Formulation of the Mechanism

The flap (link 2) is the ADGF link shown in Fig. 10. There are two pin-in-slot joints at G and F and the circular tracks are concentric with the common center A_0. A_0 is a remote center of motion and A_0A portion can be considered as a hypothetical part of the flap (that is why A_0A and A_0B_0 portions are shown as dashed lines). D is the center of mass of link 2. A nut (link 4) is attached to the flap via a revolute joint at A and the location of the nut is altered via a threaded screw B_0B (link 3). When the relative motion between the links is examined, it is seen that the A_0B_0A kinematic loop defines an inverted slider-crank mechanism.

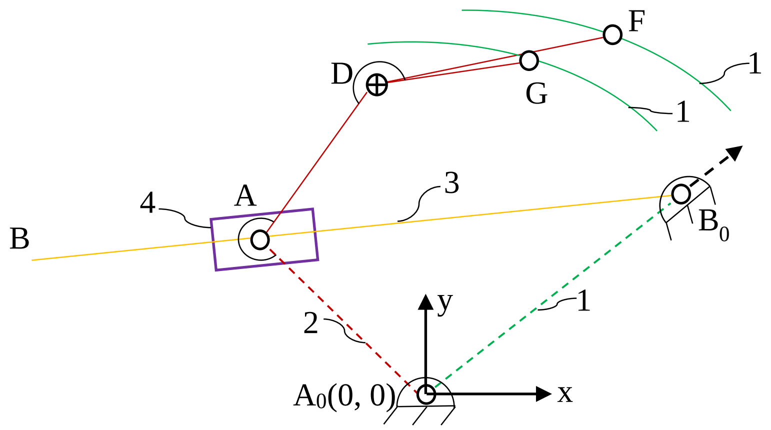

Figure 10. The mechanism representation for mobility analysis

The general DoF equation can be used (Söylemez, 2018) to calculate degree of freedom (DoF), F, of the mechanism:

$$F = \lambda(l - j - 1) + \sum_{i=1}^{j} f_i$$

where λ: DoF of space, l: the number of links, j: the number of joints, f_i: DoF of joint i.

The mechanism in Fig. 10 is planar, has four links and five joints: a revolute (R) joint between links 1 and 3 at B_0, a R joint between links 2 and 4 at A, a prismatic (P) joint between links 3 and 4 at A, two pin-in-slot (C_s) joints between links 1 and 2 at F and G. Note that the circular arcs are parts of the fixed link 1. Thus, DoF of the mechanism can be calculated as follows:

$$3(4-5-1)+3(1)+2(2)=1$$

The inverted slider-crank mechanism kinematic model is shown in Fig. 11. Counter-clockwise (CCW) direction is positive for angles. The link lengths are $|A_0B_0| = a_1$, $|A_0A| = a_2$, $|B_0B| = a_3$, $\angle xA_0B_0 = \alpha_0$ and joint variables are $|B_0A| = s_{34}$ (input), $\angle B_0A_0A = \theta_{12}$, $\angle A_0B_0B = \pi - \theta_{13}$.

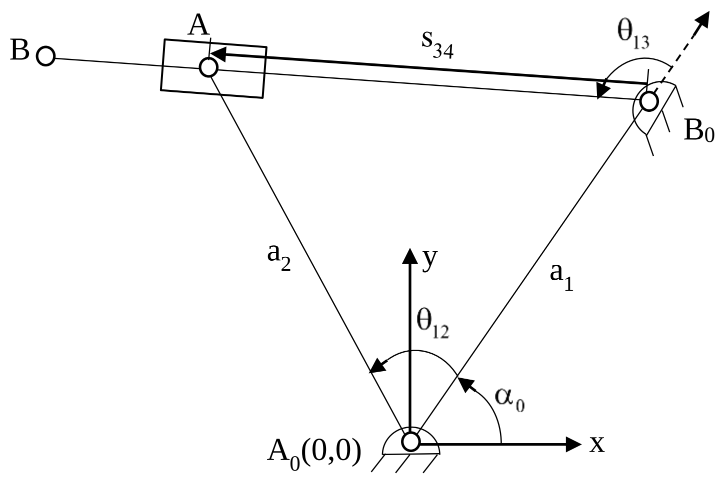

Figure 11. Inverted slider crank mechanism that actuates the flap

θ_{12} and θ_{13} can be solved using cosine theorem for given s_{34}:

$$s_{34}^2 = a_1^2 + a_2^2 - 2a_1a_2\cos\theta_{12} \Rightarrow \theta_{12} = \cos^{-1}\left(\frac{a_1^2 + a_2^2 - s_{34}^2}{2a_1a_2}\right) \quad (3.1.1)$$

$$a_2^2 = a_1^2 + s_{34}^2 - 2a_1s_{34}\cos(\pi - \theta_{13}) \Rightarrow \theta_{13} = \pi - \cos^{-1}\left(\frac{a_1^2 + s_{34}^2 - a_2^2}{2a_1s_{34}}\right) \quad (3.1.2)$$

i and f subscripts stand for "initial" and "final", respectively. In order to obtain the rotation range of the flap ($\Delta\theta_{12}$), the initial $s_{34,i}$ value should be selected, which yields $\theta_{12,i}$ and $\Delta\theta_{12} = \theta_{12} - \theta_{12,i}$ in turn as s_{34} varies. The x and y coordinates of joint locations can be calculated as follows:

$$A_0 = (0,0)$$
$$B_0 = (a_1 \cos\alpha_0, a_1 \sin a_0)$$
$$A = (a_2 \cos(\alpha_0 + \theta_{12}), a_2 \sin(\alpha_0 + \theta_{12}))$$
$$B = (B_{0,x} + a_3 \cos(\alpha_0 + \theta_{13}), B_{0,y} + a_3 \sin(\alpha_0 + \theta_{13}))$$

3.2. Parameters Defining the Slots

The two pins trace circular paths in the slots as the flap rotates, where F_1 and F_2 points in Fig. 12 represent the terminal points of the larger (b_1) and smaller (c_1) slots, respectively. Let $|A_0F_1| = b_1$, $|A_0F_2| = c_1$, $\angle xA_0F_{1,i} = \beta_1$, $\angle F_{1,i}A_0F_{2,i} = \beta_2$ and $\angle F_{1,i}A_0F_{1,f} = \angle F_{2,i}A_0F_{2,f} = \beta_3$. Then, the polar coordinates of the terminal points are: $F_{1,i} = (b_1, \beta_1)$, $F_{1,f} = (b_1, \beta_1 + \beta_3)$, $F_{2,i} = (c_1, \beta_1 + \beta_2)$ and $F_{2,f} = (c_1, \beta_1 + \beta_2 + \beta_3)$.

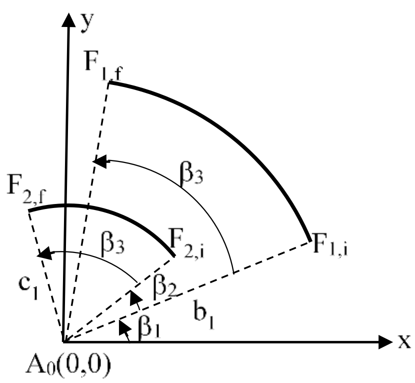

Figure 12. Circular paths of slot legs

F_1 and F_2 points are rotated about A_0 by an amount of $\Delta\theta_{12}$, which can be β_3 at most. The circular paths shown in Fig 12 are obtained by connecting these points of F_1 and F_2 for a complete rotation.

3.3. Position, Velocity and Acceleration Level Analyses of the Mechanism

In the solutions of static and dynamic force analyses, position and velocity level analyses are common in a sense, however, acceleration level analysis is required additionally for dynamic force analysis. All these analyses are done, in this section.

Loop closure equation for the inverted slider crank shown in Fig. 11:

$$a_2 e^{i(\alpha_0+\theta_{12})} = a_1 e^{i(\alpha_0)} + s_{34} e^{i(\alpha_0+\theta_{13})}$$

Velocity level analysis can be done by taking the time derivative of loop closure equation:

$$i a_2 e^{i(\alpha_0+\theta_{12})}\omega_{12} = \dot{s}_{34} e^{i(\alpha_0+\theta_{13})} + i s_{34} e^{i(\alpha_0+\theta_{13})}\omega_{13}$$

Multiply both sides by $e^{-i(\alpha_0+\theta_{13})}$:

$$i a_2 e^{i(\theta_{12}-\theta_{13})}\omega_{12} = \dot{s}_{34} + i s_{34}\omega_{13}$$

Writing real and imaginary parts and solving for ω_{12} and ω_{13}:

$$-a_2 \sin(\theta_{12}-\theta_{13})\omega_{12} = \dot{s}_{34} \Rightarrow \omega_{12} = \frac{\dot{s}_{34}}{a_2 \sin\left(\theta_{13}-\theta_{12}\right)} \qquad (3.3.1)$$

$$a_2 \cos(\theta_{12}-\theta_{13})\omega_{12} = s_{34}\omega_{13} \Rightarrow \omega_{13} = \frac{a_2 \cos(\theta_{12}-\theta_{13})\omega_{12}}{s_{34}} = \frac{\dot{s}_{34}}{s_{34} \tan\left(\theta_{13}-\theta_{12}\right)} \qquad (3.3.2)$$

Acceleration level analysis can be done by differentiating the velocity expressions:

$$\omega_{12} = \frac{\dot{s}_{34}}{a_2 \sin\left(\theta_{13}-\theta_{12}\right)} \Rightarrow \alpha_{12} = \frac{\tan\left(\theta_{13}-\theta_{12}\right)\ddot{s}_{34} - (\omega_{12}-\omega_{13})\dot{s}_{34}}{a_2 \sin\left(\theta_{13}-\theta_{12}\right)\tan\left(\theta_{13}-\theta_{12}\right)} \qquad (3.3.3)$$

$$\omega_{13} = \frac{\dot{s}_{34}}{s_{34} \tan\left(\theta_{13}-\theta_{12}\right)} \Rightarrow \alpha_{13} = \frac{s_{34}\ddot{s}_{34} - \dot{s}_{34}^2}{s_{34}^2 \tan\left(\theta_{13}-\theta_{12}\right)} - \frac{(\omega_{13}-\omega_{12})\dot{s}_{34}}{s_{34} \sin^2\left(\theta_{13}-\theta_{12}\right)} \qquad (3.3.4)$$

3.4. Static Force Analysis of the Mechanism

To carry out static and dynamic (if necessary) force analyses, Fig. 13 includes, point D as flap' center of mass, points G and F as flap legs' contact points on slots.

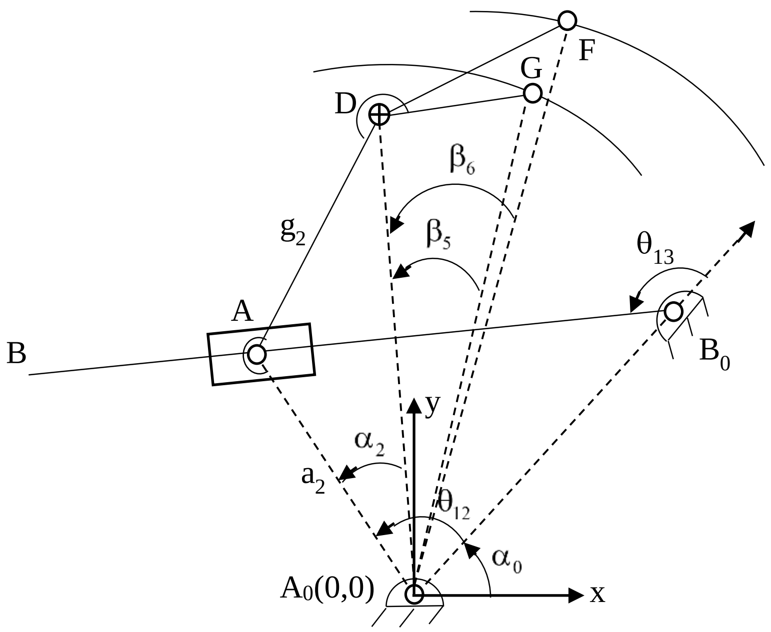

Figure 13. Inverted slider crank mechanism attached to the flap

Position, velocity and acceleration of point A are required for static and dynamic force analyses while applying virtual work method and/or total power:

$$\vec{r}_A = a_2 e^{i(\alpha_0+\theta_{12})}$$
$$x_A = a_2 \cos(\alpha_0+\theta_{12}) \tag{3.4.1}$$
$$y_A = a_2 \sin(\alpha_0+\theta_{12})$$

$$\begin{aligned} \dot{x}_A &= -a_2 \sin(\alpha_0+\theta_{12})\omega_{12} \\ \dot{y}_A &= a_2 \cos(\alpha_0+\theta_{12})\omega_{12} \end{aligned} \tag{3.4.2}$$

$$\begin{aligned} \ddot{x}_A &= -a_2\left[\cos(\alpha_0+\theta_{12})\omega_{12}^2 + \alpha_{12}\sin(\alpha_0+\theta_{12})\right] \\ \ddot{y}_A &= a_2\left[-\sin(\alpha_0+\theta_{12})\omega_{12}^2 + \alpha_{12}\cos(\alpha_0+\theta_{12})\right] \end{aligned} \tag{3.4.3}$$

Assuming position of point D is known, its position, velocity and acceleration analyses can be computed as:

$$g_2 = |AD| = \sqrt{(x_D - x_A)^2 + (y_D - y_A)^2}$$

$$|r_D| = |A_0D| = \sqrt{x_D^2 + y_D^2}$$

$$g_2^2 = a_2^2 + r_D^2 - 2a_2 r_D \cos\alpha_2 \Rightarrow \alpha_2 = \angle DA_0A = \cos^{-1}\left(\frac{a_2^2 + r_D^2 - g_2^2}{2a_2 r_D}\right)$$

$$\theta_D > \alpha_0 + \theta_{12,i} \Rightarrow \sigma = 1$$
$$\theta_D \le \alpha_0 + \theta_{12,i} \Rightarrow \sigma = -1$$

$$\begin{aligned} \theta_D &= \angle xA_0D = \operatorname{atan2}(x_D; y_D) = \alpha_0 + \theta_{12} + \sigma\alpha_2 \\ x_D &= r_D \cos(\alpha_0 + \theta_{12} + \sigma\alpha_2) \\ y_D &= r_D \sin(\alpha_0 + \theta_{12} + \sigma\alpha_2) \end{aligned} \tag{3.4.4}$$

$$\begin{aligned} \dot{x}_D &= v_{Dx} = -r_D \sin(\alpha_0 + \theta_{12} + \sigma\alpha_2)\omega_{12} \\ \dot{y}_D &= v_{Dy} = r_D \cos(\alpha_0 + \theta_{12} + \sigma\alpha_2)\omega_{12} \end{aligned} \tag{3.4.5}$$

$$\begin{aligned} \ddot{x}_D &= a_{Dx} = -r_D\left[\cos(\alpha_0 + \theta_{12} + \sigma\alpha_2)\omega_{12}^2 + \alpha_{12}\sin(\alpha_0 + \theta_{12} + \sigma\alpha_2)\right] \\ \ddot{y}_D &= a_{Dy} = r_D\left[-\sin(\alpha_0 + \theta_{12} + \sigma\alpha_2)\omega_{12}^2 + \alpha_{12}\cos(\alpha_0 + \theta_{12} + \sigma\alpha_2)\right] \end{aligned} \tag{3.4.6}$$

Note: σ(=+1 or -1) indicates whether α_2 is added to $\angle xA_0A=\alpha_0+\theta_{12}$ or subtracted from that angle according to position of point D.

θ_F and θ_G angles can be found using β_5 and β_6 shown in Fig. 12, which are required for force calculations. β_5 and β_6 can be found using $F_{1,i}$ and $F_{2,i}$ for the closed configuration of flap:

$$p_2 = |DG| = \sqrt{(F_{2,ix} - x_D)^2 + (F_{2,iy} - y_D)^2}$$

$$q_2 = |DF| = \sqrt{(F_{1,ix} - x_D)^2 + (F_{1,iy} - y_D)^2}$$

$$\beta_5 = \cos^{-1}\left(\frac{r_D^2 + c_1^2 - p_2^2}{2r_Dc_1}\right)$$

$$\beta_6 = \cos^{-1}\left(\frac{r_D^2 + b_1^2 - q_2^2}{2r_Db_1}\right)$$

$$\theta_G = \angle xA_0G = \theta_D - \beta_5$$
$$\theta_F = \angle xA_0F = \theta_D - \beta_6$$

Problem: Given M_{12}, the moment (resultant moment of drag and lift forces on one flap) which tends to close the mechanism, find $M_{opening/raise}$ (M_o) for flap deployment and $M_{closing/lower}$ (M_c) for flap retraction. Note, although the actuation is provided via a screw jack, the solution is developed for piston-cylinder actuation to obtain input force, which is going to be used in screw jack torque requirement at a later stage.

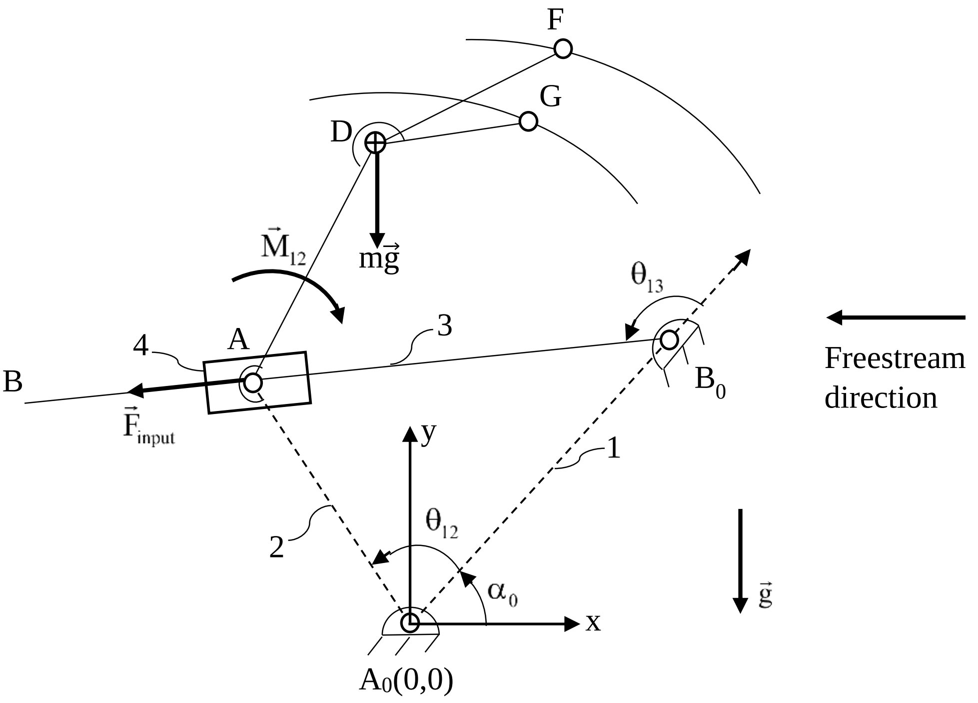

Figure 14. Moments and forces acting on mechanism (circular arc' radii and arc angles are representative)

According to the acceleration level analyses of points A and D, inertia forces are found to be negligible (see Fig. 31). This is seen after comparing the acceleration values, a_A and a_D, with gravitational acceleration (g) value for a given set of proper parameter values, which are computed to be about 0.1%. Thus, they are omitted in force calculations. Assumptions:

- Assuming that there is sufficient amount of lubrication, frictional forces at the revolute joints are omitted to keep the model simple.
- All links and joints are rigid.
- The masses of the links except the flap link are negligible.
- The mechanism plane makes negligibly small angles (as much as wing angles, explained in Chapter 4) with gravity direction (–Y) such that projection of $m\vec{g}$ is not only on –Y direction, however, g is assumed to be on –Y direction. See Appendix B.

Free body diagrams are drawn (Figs. 15-16) to derive force and moment equilibrium equations.

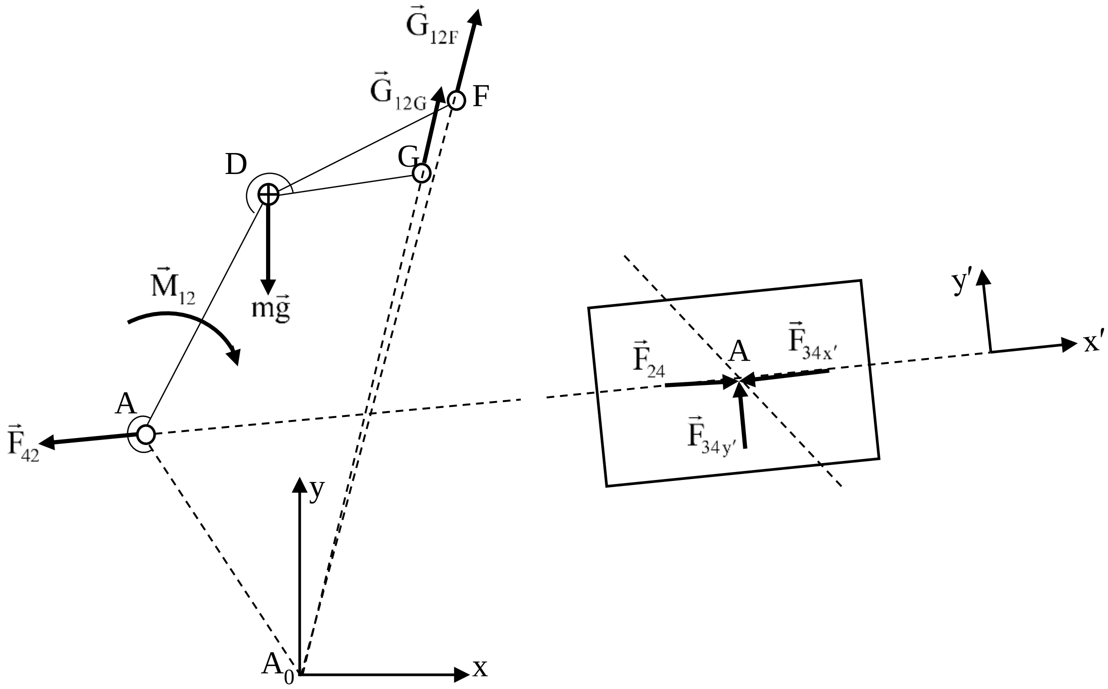

Figure 15. Free body diagrams for links 2 and 4

For link 2:

$$\sum M_{A_0} = mgr_D \sin\left(\tfrac{3\pi}{2} - \theta_D\right) + F_{42} a_2 \sin\left(\theta_{13} - \theta_{12}\right) - M_{12} = 0 \qquad (3.4.7)$$

$$\sum F_x = G_{12G} \cos\theta_G + G_{12F} \cos\theta_F + F_{42} \cos\left(\alpha_0 + \theta_{13}\right) = 0 \qquad (3.4.8)$$

$$\sum F_y = G_{12G} \sin\theta_G + G_{12F} \sin\theta_F + F_{42} \sin\left(\alpha_0 + \theta_{13}\right) - mg = 0 \qquad (3.4.9)$$

The actuation force is $F_{34x'} = F_{input}$. For link 4:

$$\vec{F}_{24} = -\vec{F}_{42} \qquad (3.4.10)$$

$$\sum F_{x'} = F_{24} - F_{input} = 0 \qquad (3.4.11)$$

$$\sum F_{y'} = F_{34y'} = 0 \qquad (3.4.12)$$

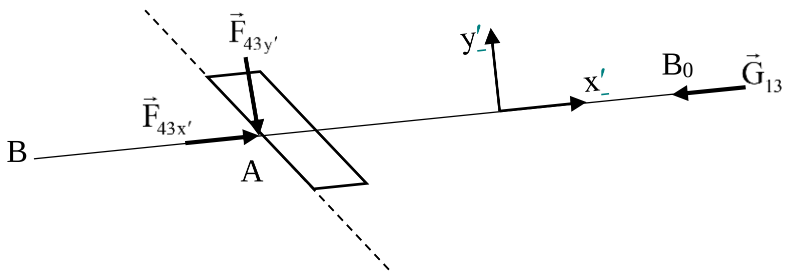

Figure 16. Free body diagram for link 3

For link 3:

$$\vec{F}_{34x'} = -\vec{F}_{43x'} \tag{3.4.13}$$

$$\sum F_{y'} = F_{43y'} = 0 \tag{3.4.14}$$

$$\sum F_{x'} = F_{43x'} - G_{13} = 0 \tag{3.4.15}$$

Solve F_{42} using equations (3.4.7), (3.4.10) and (3.4.11):

$$F_{42} = F_{24} = F_{input} = \frac{M_{12} - mgr_D \sin\left(\frac{3\pi}{2} - \theta_D\right)}{a_2 \sin\left(\theta_{13} - \theta_{12}\right)} = \frac{M_{12} + mgr_D \cos\theta_D}{a_2 \sin\left(\theta_{13} - \theta_{12}\right)} \tag{3.4.16}$$

Rewriting equations (3.4.8) and (3.4.9) in matrix form:

$$\begin{bmatrix} \cos\theta_G & \cos\theta_F \\ \sin\theta_G & \sin\theta_F \end{bmatrix} \begin{bmatrix} G_{12G} \\ G_{12F} \end{bmatrix} = \begin{bmatrix} -F_{42}\cos\left(\alpha_0 + \theta_{13}\right) \\ mg - F_{42}\sin\left(\alpha_0 + \theta_{13}\right) \end{bmatrix}$$

Using Cramer's rule:

$$G_{12G} = \frac{\begin{vmatrix} -F_{42}\cos\left(\alpha_0 + \theta_{13}\right) & \cos\theta_F \\ mg - F_{42}\sin\left(\alpha_0 + \theta_{13}\right) & \sin\theta_F \end{vmatrix}}{\begin{vmatrix} \cos\theta_G & \cos\theta_F \\ \sin\theta_G & \sin\theta_F \end{vmatrix}} = \frac{F_{42}\sin\left(\alpha_0 + \theta_{13} - \theta_F\right) - mg\cos\theta_F}{\sin\left(\theta_F - \theta_G\right)}$$

$$G_{12F} = \frac{\begin{vmatrix} \cos\theta_G & -F_{42}\cos\left(\alpha_0 + \theta_{13}\right) \\ \sin\theta_G & mg - F_{42}\sin\left(\alpha_0 + \theta_{13}\right) \end{vmatrix}}{\begin{vmatrix} \cos\theta_G & \cos\theta_F \\ \sin\theta_G & \sin\theta_F \end{vmatrix}} = \frac{mg\cos\theta_G - F_{42}\sin\left(\alpha_0 + \theta_{13} - \theta_G\right)}{\sin\left(\theta_F - \theta_G\right)}$$

Using equations (3.4.10), (3.4.11), (3.4.13) and (3.4.15):

$$\vec{F}_{input} = \vec{F}_{34x'} = -\vec{F}_{24} = \vec{F}_{42} = -\vec{F}_{43x'} = \vec{G}_{13}$$

Using equations (3.4.12) and (3.4.14):

$$F_{34y'} = F_{43y'} = 0$$

3.5. Force Analysis Using Total Power

Total power:

$$P_{total} = \vec{M}_{12} \cdot \vec{\omega}_{12} + m\vec{g} \cdot \vec{v}_D + \vec{F}_{input} \cdot \vec{v}_A = -M_{12}\omega_{12} - mg\dot{y}_D + F_{input}\dot{s}_{34} = 0$$

Using equations (3.3.1), (3.4.2), (3.4.4) and (3.4.5):

$$\left[-M_{12} - mgr_D \cos\theta_D + F_{input} a_2 \sin(\theta_{13} - \theta_{12})\right]\omega_{12} = 0$$

The term inside the parenthesis should be zero, so:

$$F_{input} = \frac{M_{12} + mgr_D \cos\theta_D}{a_2 \sin(\theta_{13} - \theta_{12})} \tag{3.5.1}$$

Notice that equations (3.4.16) and (3.5.1) are equivalent. In the next section, the required screw torque to raise and lower (to open and close) the flap are found.

3.6. Screw Jack Torque Requirement

To actuate the flap mechanism while enduring the drag-lift forces/moments developing on the flap, a torque input is given from a screw jack. To determine the required torque input value, inclined plane analogy can be employed between nut-screw contact since the load can be handled as infinitesimal blocks appearing along the radius of the nut, rather than a point load, modelled as normal forces, frictions and torques. A square threaded screw is shown below in Fig. 17 (Hibbeler, 2009; Budynas & Nisbett, 2006).

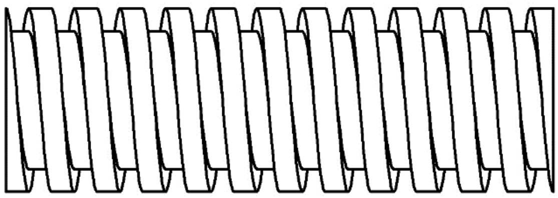

Figure 17. Portion of a square-threaded screw

If one revolution of the threaded portion is unwrapped on a plane, it can be represented as in Fig. 18 and accordingly, inclined plane analogy is used. Here, r is the mean radius of the screw, λ is the lead angle, l is the lead, $\vec{N}$ is the normal force, f is thread friction coefficient, $\vec{L}$ is the axial load, $\vec{T}_R$ is the raising torque and $F_R = T_R/r$. In the literature, the actuation torques are called raising torque ($\vec{T}_R$) and lowering torque ($\vec{T}_L$), because typical applications of lead screws are to raise and lower the loads.

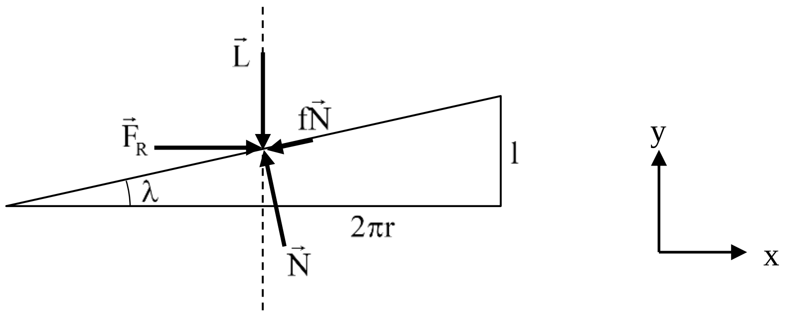

Figure 18. Free body diagram to examine torque to raise the load

Force equilibrium equations for Fig. 18:

$$\sum F_x = F_R - fN\cos\lambda - N\sin\lambda = 0 \tag{3.6.1}$$

$$\sum F_y = -L - fN\sin\lambda + N\cos\lambda = 0 \tag{3.6.2}$$

Solving N from (3.6.2):

$$N = \frac{L}{\cos\lambda - f\sin\lambda} \tag{3.6.3}$$

Using (3.6.3) in (3.6.1) to solve for the torque T_R:

$$T_R = rF_R = \frac{r\left(f + \tan\lambda\right)}{1 - f\tan\lambda}L \tag{3.6.4}$$

The free body diagram in the case of lowering is presented in Fig. 19.

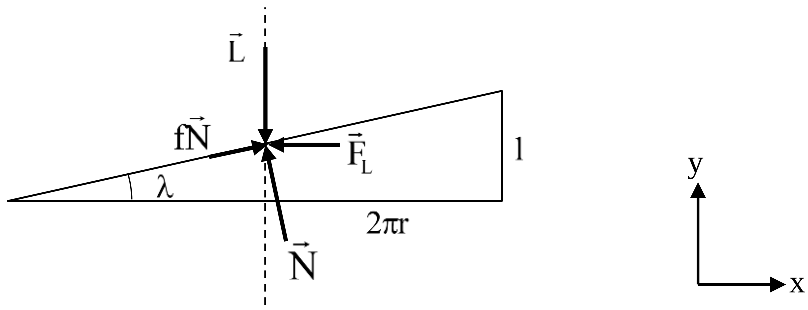

Figure 19. Free body diagram to examine torque to lower the load

Force equilibrium equations for Fig. 19:

$$\sum F_x = -F_L + fN\cos\lambda - N\sin\lambda = 0 \tag{3.6.5}$$

$$\sum F_y = -L + fN\sin\lambda + N\cos\lambda = 0 \tag{3.6.6}$$

Solving N from (3.6.6):

$$N = \frac{L}{f\sin\lambda + \cos\lambda} \tag{3.6.7}$$

Using (3.6.7) in (3.6.5) to solve for the torque T_L:

$$T_L = rF_L = \frac{r(f - \tan\lambda)}{1 + f\tan\lambda} L \qquad (3.6.8)$$

Since $\tan\lambda = l/2\pi r$, rewrite (3.6.4) and (3.6.8) as:

$$T_R = \left(\frac{2\pi r f + l}{2\pi r - f l}\right) rL \qquad (3.6.9)$$

$$T_L = \left(\frac{2\pi r f - l}{2\pi r + f l}\right) rL \qquad (3.6.10)$$

For the flap mechanism, the load $\vec{L}$ is the $\vec{F}_{input}$. Therefore, corresponding opening and closing torque values can be found using the (3.6.9) and (3.6.10), respectively.

CHAPTER 4

DESIGN METHODOLOGY

Typically, flaps are actuated via more than one mechanism which work on different planar sections. The parametric model presented in Chapter 3 can be used for a plane, where the flap size and drag-lift forces/moment values are known. The methodology presented in this Chapter is applied on an outer flap mechanism of an aircraft, equipped with one flap on a wing which is actuated via two flap mechanisms, and then inner one is generated by translating the outer one with the same parameter set. Since the wing has a trapezoidal geometry (Fig. 20), section for outer flap mechanism is narrower and may have less allowable portion than the inner one. Accordingly, any result generated on outer section may be safely adapted to inner section.

A 3D wing geometry and several wing planforms, seen in Fig. 20-21, help to visualize the wing angles and define related wing parameters according to (Houghton et al., 2017).

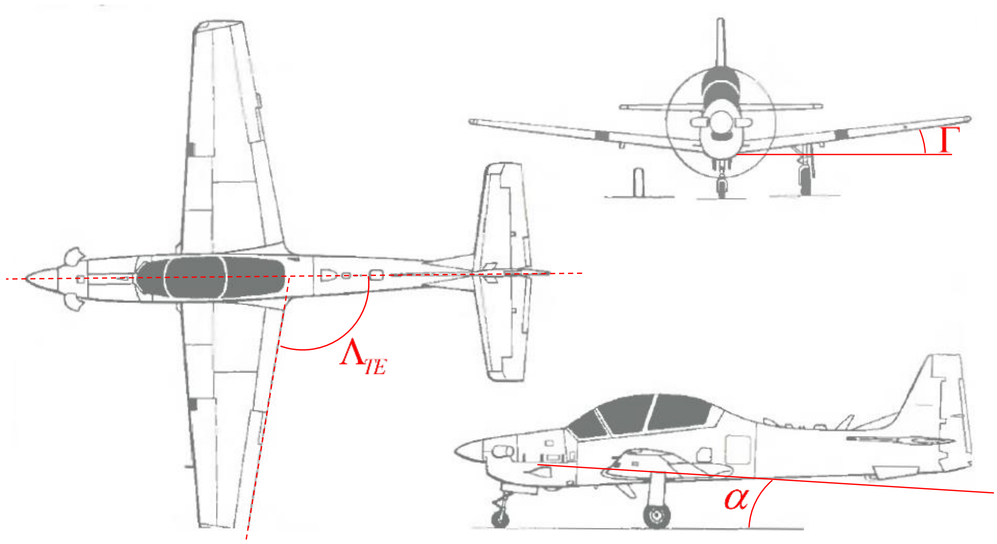

Figure 20. Three view of a small aircraft (Source: Jackson, 2004)

The following parameters are used in Fig. 21:

Wingspan (b): Wing tips’ distance.

Sweep angle (Λ): The angle measured from the leading edge (Λ_{LE}), from the quarter-chord line (from leading edge) ($\Lambda_{1/4}$) or from the trailing edge (Λ_{TE}) which is seen in Fig. 20.

Dihedral/Anhedral angle (Γ): The angle between wing and horizontal while looking the aircraft from front, seen in Fig. 20. It is called dihedral if the wing is inclined upwards, it is called anhedral if the wing is inclined downwards.

Wing twist: Geometric angle of attack (α) is the angle between airfoil chord and the direction of flight. Airfoil cross sections along wingspan have different geometric angle of attacks for twisted wings. Wings are named wash-in/wash-out if they have increasing/decreasing angle of attack values towards their tips, respectively.

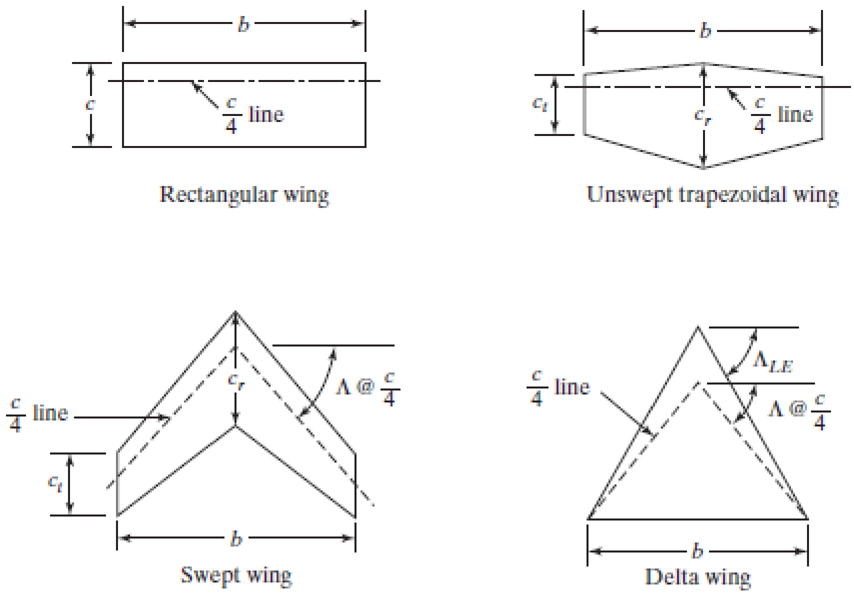

Figure 21. Several wing planforms (Source: Bertin & Cummings, 2014)

The methodology presents determining the flap mechanism planes, creation of slots, mechanism and flap link step by step below. The components of the mechanism and its actuator should not interfere with the wing and its components, throughout the implementation of steps. The airfoil type of the flap in Fig. 22 is NACA 63(1)-212 (NACA 63-212 AIRFOIL (N63212-il), n.d.) and is used to illustrate the following steps to determine the mechanism planes:

Step 1) Since rotation axis of flap and flap size are known, inner flap plane (inner side surface of the flap) is intersected with the rotation axis of the flap to obtain point P (Fig. 22). The inner flap plane, in general, is not perpendicular to the flap rotation axis.

Step 2) A_0 is located by translating P by amount of d_1 along the rotation axis, towards the outer side of the flap. Then, the outer flap mechanism plane is defined as the plane passing through A_0 and perpendicular to the flap rotation axis. A local coordinate frame $A_0(xyz)$ is defined such that z-axis is along the flap rotation axis, the x-axis is perpendicular to the gravity direction (–Y direction in Fig. 22) and heading towards the nose of the plane. See Appendix A for three views of the flap to visualize the wing angles.

Step 3) Translate $A_0(xyz)$ by an amount of d_2 (d_2 should be less than the flap span), to locate $A_1(x_1y_1z_1)$ as the origin of the inner mechanism plane local frame (Fig. 22).

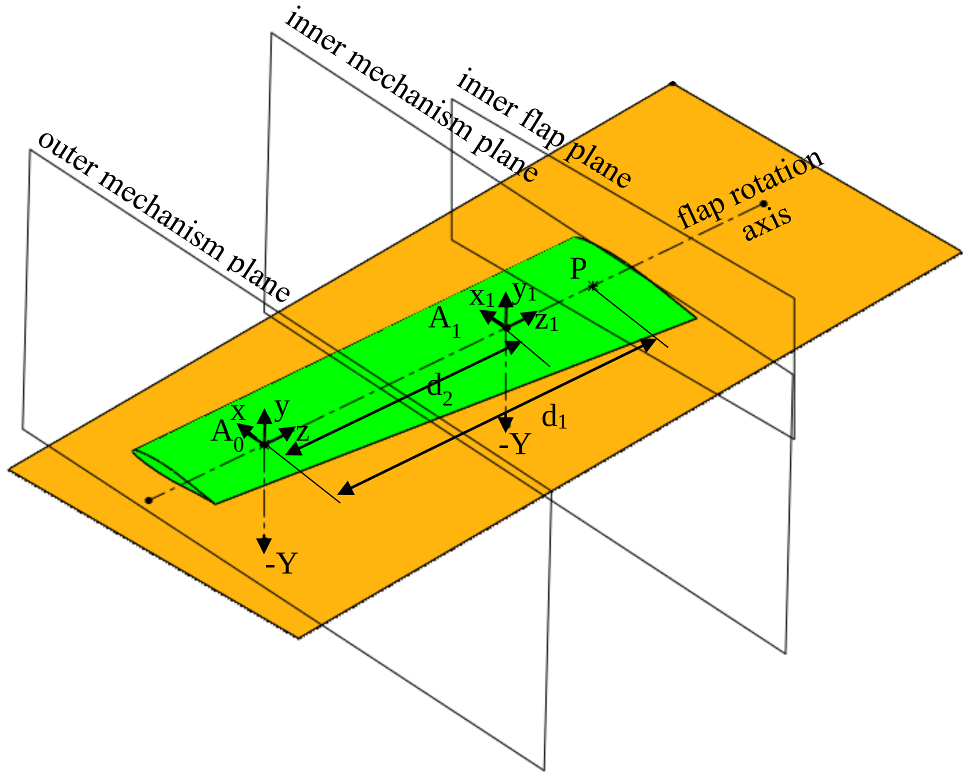

Figure 22. Mechanism planes for the flap at left wing (port wing) (the flap and ground are colored in green and brown, respectively)

To create the slots:

Step 4) The radii of the two concentric circular arcs and the common center A_0 are selected ($b_1 > c_1$ in Fig. 12). The arcs should not interfere with the flap, wing and their components and remain inside the wing as much as possible.

Step 5) The arc angles (flap rotation range: β_3) are selected for both arcs. Also, β_1 and β_2 angles are selected to specify the terminal points of the arcs (see Fig. 12).

To create the mechanism:

Step 6) Locate B_0 by selecting a_1 and α_0 (see Fig. 11) such that it is close to the region between the terminal points of the arcs, which are close to inner side of the wing.

Step 7) B_0 is the fixed end of the lead screw, orientation of which is determined by selecting a_2 in Fig. 11. Since point A traces a circle with radius a_2 by an amount of β_3 rotation around A_0, an isosceles triangle $\Delta A_0A_iA_f$ is formed as shown in Fig. 23. Select an a_2 value (β_3 is already selected in Step 5). Also, $\Delta s = |s_{34,f} - s_{34,i}| = |A_iA_f|$ can be found as $\Delta s = 2a_2\sin(\beta_3/2)$.

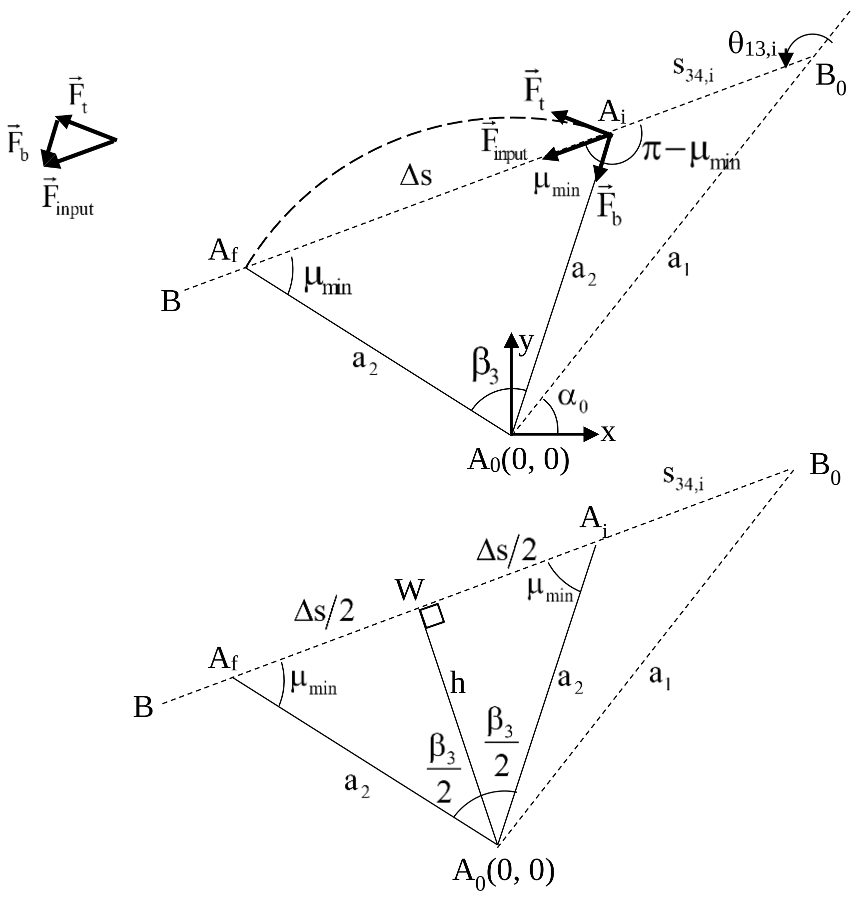

Figure 23. Drawing for design methodology

Step 8) Select A_i and A_f, such that B_0A_i and B_0A_f are collinear as shown in Fig. 23. This collinearity ensures that the deviation of transmission angle (μ) from 90° becomes minimum. The transmission angle is the angle between A_0A (the flap) and the lead screw (B_0B) as shown in Fig. 23 where, $\vec{F}_{input}$ is the transmitted force to the flap link, $\vec{F}_t$ is the force creating a moment about A_0 and $\vec{F}_b$ causes joint reaction forces at the slots. Accordingly, the critical minimum transmission angle is $\mu_{min} = (\pi - \beta_3)/2$. Besides, $s_{34,i}$ can be determined. For $|A_0W| = h = a_2\cos(\beta_3/2)$ and $t = \Delta s/2 + s_{34,i} = a_2\sin(\beta_3/2) + s_{34,i}$:

$$a_1^{\,2} = a_2^{\,2}\cos^2\left(\beta_3/2\right) + t^2 \Rightarrow t = \sqrt{a_1^{\,2} - a_2^{\,2}\cos^2\left(\beta_3/2\right)} \Rightarrow s_{34,i} = t - a_2\sin\left(\beta_3/2\right)$$

Accordingly, Cartesian coordinates of A_i and A_f are found as:

$$A_i = \left(a_1\cos\alpha_0 + s_{34,i}\cos\left(\alpha_0 + \theta_{13,i}\right), a_1\sin\alpha_0 + s_{34,i}\sin\left(\alpha_0 + \theta_{13,i}\right)\right)$$

$$A_f = \left(a_1\cos\alpha_0 + \left(\Delta s + s_{34,i}\right)\cos\left(\alpha_0 + \theta_{13,i}\right), a_1\sin\alpha_0 + \left(\Delta s + s_{34,i}\right)\sin\left(\alpha_0 + \theta_{13,i}\right)\right)$$

Step 9) Select a_3 to be slightly greater than $\Delta s + s_{34,i}$.

To create the flap link:

Step 10) Joints of the flap are located at points A, G and F (G and F are the pins on the circular slots in Fig. 10). Each of these points are connected to point D, representing the center of mass of the flap, position of which is assumed to be known. Then, $|AD| = g_2$, $|DG| = p_2$ and $|DF| = q_2$ parameters are determined (they are used for the force analysis).

CHAPTER 5

CASE STUDY FOR A SMALL AIRCRAFT

In this Chapter, the model and design methodology presented in Chapters 3 and 4 are applied for a small size aircraft having two flap mechanisms on its each wing as a case study. Besides, this application is provided in 2D, cross-sectional view of corresponding wing plane, and is applied only rear part of the wing, including the rear spar. The aim is to locate these flap mechanisms and actuation systems on the wing such that the fairing size will be smaller than the dropped-hinge type mechanism and hence the fairing drag will be reduced during flight.

5.1. Parameter Set

Design constraints:

- Flap must rotate about a specified axis by 35°.
- Fairing size must be kept minimum.
- Throughout the deployment, the mechanism and the actuation system should not interfere with the flap and the wing. For instance, the big black dot seen in Fig. 24 represents the torque tube, which cannot be interfered.
- Slots can penetrate up to the flap spar (structural element between upper and lower surfaces of the airfoil seen in Fig. 24,) which is located about 20 percent chord of flap from its leading edge.

Design considerations:

- The transmission angle of the mechanism should be optimized to achieve better force transmission and lower joint forces.
- The screw jacks can be located in between two flap mechanism sections, therefore, any collision of screw jacks with the slots is not a problem which can be misinterpreted if any collision occurs in cross-sectional figures.

5.2. Application of the Methodology

To determine the mechanism planes, steps 1, 2 and 3 are presented in Appendix B (d_1 and d_2 are not indicated, their orientations are determined only). To create the slots:

Step 4) The radii of the two concentric circular arcs are selected as b_1 = 350 mm and c_1 = 300 mm and their common center is A_0 (origin) (Fig. 24).

Figure 24. Drawing for step 4

Step 5) The arc angles (flap rotation range: β_3) are selected as β_3 = 35° for both arcs. Also, β_1 = 40° and β_2 = 20° angles are selected to specify the terminal points of the arcs (Fig. 25).

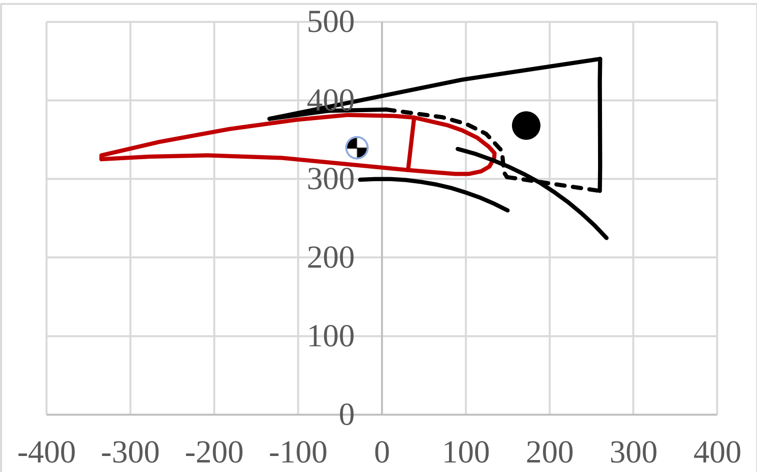

Figure 25. Drawing for step 5

To design the mechanism:

Step 6) Locate B_0 such that a_1 = 275 mm and α_0 = 65° (Fig. 26).

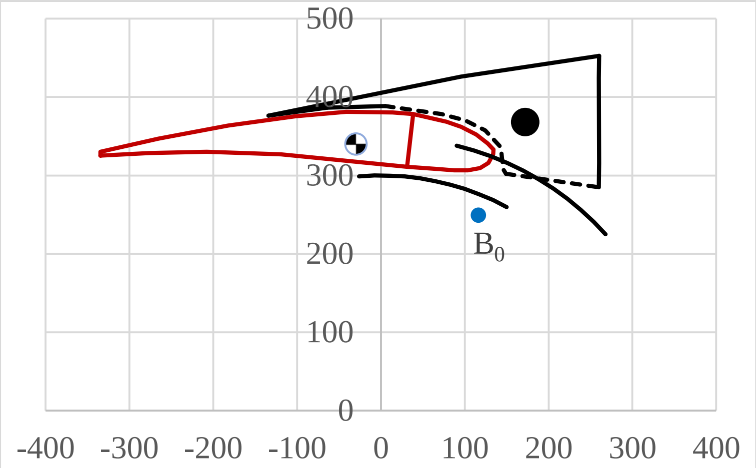

Figure 26. Drawing for step 6

Step 7) Select a_2 = 240 mm. The isosceles triangle $A_0A_iA_f$ is free to rotate about A_0. Similarly, the lead screw's fixed end is free rotate about B_0 (Fig. 27).

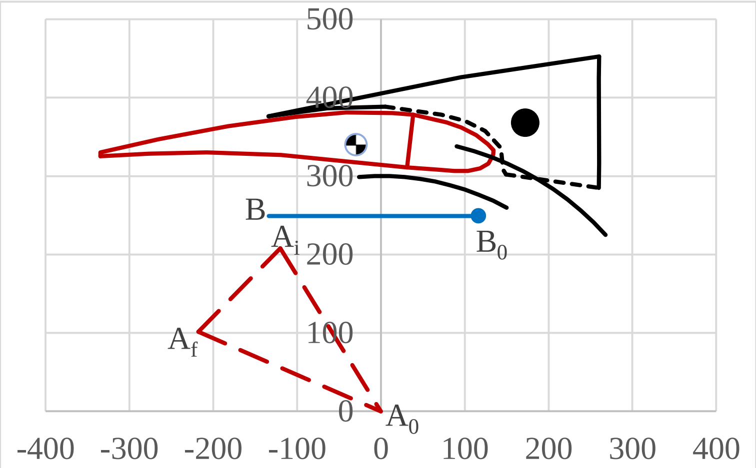

Figure 27. Drawing for step 7

Step 8) The collinearity of B_0, A_i and A_f results in $s_{34,i}$ = 80.3 mm (Fig. 28).

Step 9) Select a_3 as a_3 = 250 mm > 144.3 + 80.3 mm.

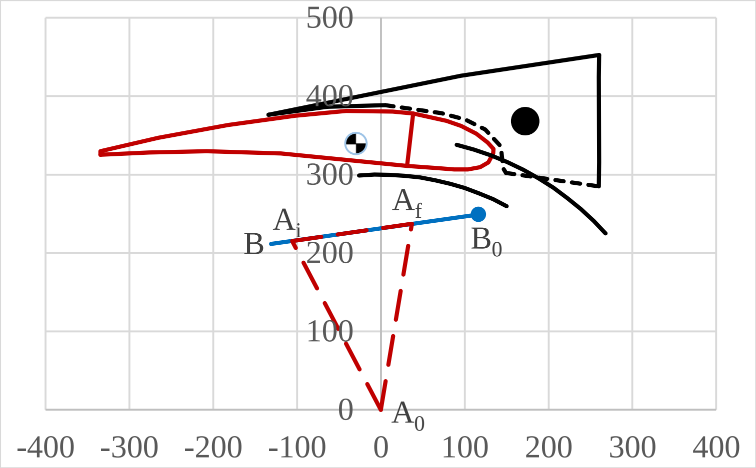

Figure 28. Drawing for step 8

To create the flap link:

Step 10) When the flap is closed, the coordinates of D are (–30, 340). So, $|AD| = g_2 = 122.7$ mm, $|DG| = p_2 = 197.1$ mm and $|DF| = q_2 = 319.5$ mm (Fig. 29).

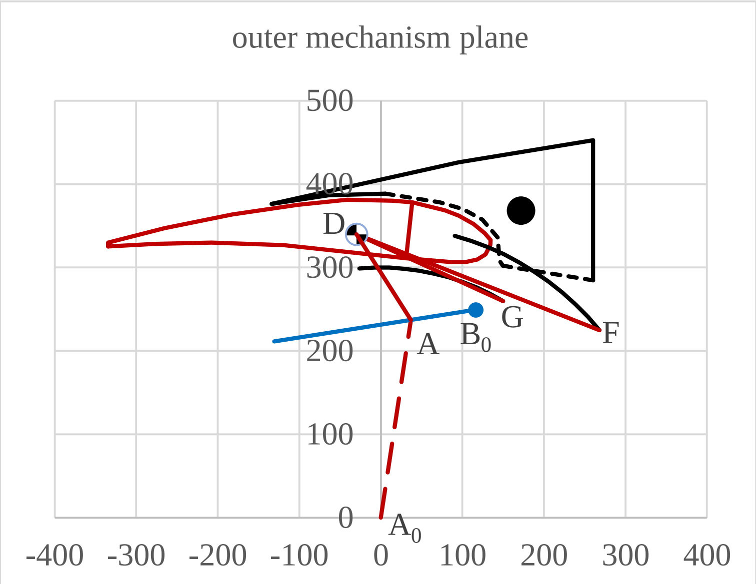

Figure 29. Drawing for step 10

The mechanism generation is completed for the parameter set listed in Table 2 where, the screw parameters as expressed in Section 3.6 are; l = 8 mm, r = 16 mm and f is assumed to be 0.1, according to (Ugural, 2015). The resulting mechanism is shown in Fig. 30. In Table 2, yellow and green parameters represent variable parameters and computed parameters, respectively. Thus, a_1, a_2, α_0, b_1, c_1, β_1, β_2, β_3 may be varied in Excel to alter the solution in Fig 30, which may further reduce fairing depth. Since fairing depth of dropped-hinge mechanism would be up to A_0, fairing depth is reduced approximately by an amount of h (see Fig. 23) with the presented solution. Additionally, the screw jack can deploy the flap to any arbitrary position between closed and fully deployed configurations more precisely than a hydraulic piston (Screw Jack Introduction, n.d.).

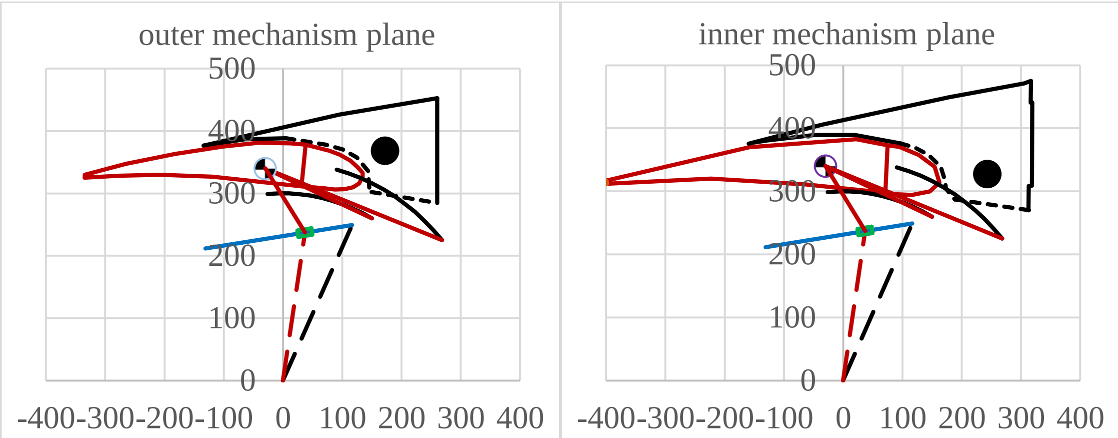

Figure 30. Outer and inner mechanism planes

Table 2. Parameter set for case study

a_1	275 mm	b_1	350 mm	x_D	–30 mm	r	16 mm
a_2	240 mm	c_1	300 mm	y_D	340 mm	l	8 mm
a_3	250 mm	β_1	40°	g_2	122.7 mm	f	0.1
$s_{34,i}$	80.3 mm	β_2	20°	p_2	197.1 mm	$\dot{s}_{34}$	35 mm/s
Δs	144.3 mm	β_3	35°	q_2	319.5 mm	$\ddot{s}_{34}$	0 mm/s^2
α_0	65°	m_{flap}	12 kg	α_2	14°	g	9.81 m/s^2

The accelerations of points A and D are computed throughout the flap deployment, for the constant input speed of nut $\dot{s}_{34}$ = 35 mm/s, $\ddot{s}_{34}$ = 0 mm/s^2 as in Fig. 31 and it is seen that the accelerations are less than 0.1% of the gravitational acceleration g. Accordingly, inertia forces can be neglected as stated in Section 3.4.

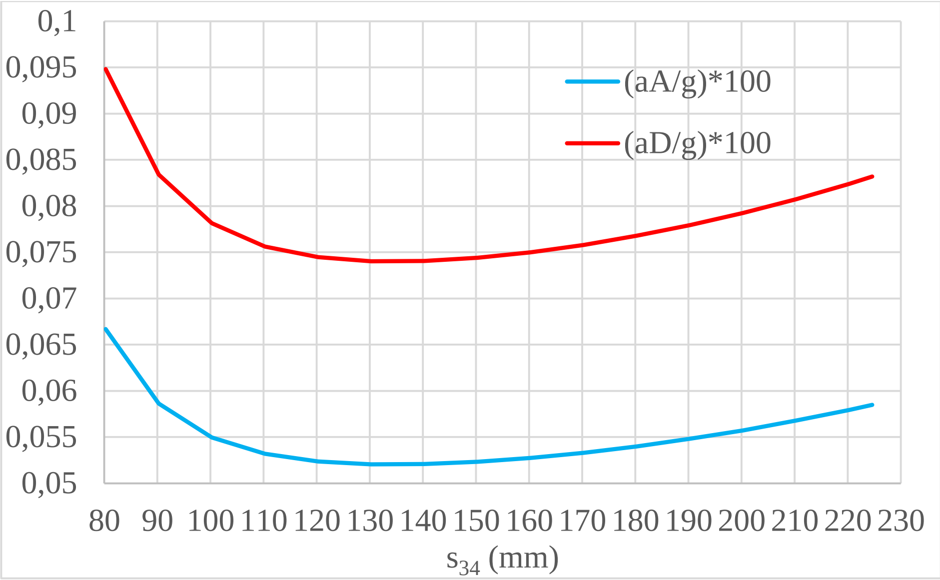

Figure 31. Percentage acceleration ratios of points A and D over g

Since two screw jacks actuate the flap mechanism, half of the external moment (M_{12}) values stated below are used for the following flight scenarios. The plane is assumed to be parallel to the ground, so that change in the direction of the gravitational acceleration is negligible.

- Cruise scenario: M_{12} = 750 N·m when flap is closed for maximum cruise speed of the aircraft.
- Landing scenario: M_{12min} = 220 N·m when flap is closed and M_{12max} = 650 N·m when flap is fully deployed (both at landing speed). Intermediate moment values are computed via linear interpolation.

According to these scenarios, results of force analysis are summarized in Table 3.

Table 3. Results of force analysis

	Cruise scenario	Landing scenario (min/max)
$\vec{F}_{input} = \vec{F}_{34x'} = -\vec{F}_{24} = \vec{F}_{42} = -\vec{F}_{43x'} = \vec{G}_{13}$	1623 N	465 / 1307 N
G_{12G}	–2204 N	–3411 / -444 N
G_{12F}	3533 N	890 / 3843 N
$F_{34y'} = F_{43y'}$	0 N	0 / 0 N
T_R	4700 N·mm	1347 / 3785 N·mm
T_L	526 N·mm	151 / 424 N·mm

According to Table 3, required maximum motor torque is 4.7 N·m. If a safety factor of 1.5 is employed, 7.1 N·m torque is required from each screw jack for two of them. Also, negative force/moment results show that their directions should be reversed on free body diagrams. It can be noted that, screw jacks are driven by an electric motor where the torque is transmitted via torque tubes with proper transmission.

When magnitudes of M_{12} and $mgr_D\cos\theta_D$ in equation (3.5.1) are compared, to their contribution for F_{input}, the contribution of the flap weight to F_{input} does not exceed 8%, thus external moment is much more dominant than the weight.

5.3. Model Implementation in Excel

The parametric model developed in Chapter 3 is implemented in Excel (see Appendix C). If the following conditions occur on the Excel file, corresponding cells are filled in red color.

1) $s_{34} < s_{34,i}$ or $\Delta\theta_{12} > \beta_3$: s_{34} becomes red since the pins cannot move out of the slots.

2) $c_1 \geq b_1$: c_1 becomes red since c_1 is assumed to be the smaller radius.

3) $s_{34} > a_3$: a_3 becomes red since screw jack length cannot be less than slider displacement.

Slider in green represents nut, which has arbitrary dimensions.

CHAPTER 6

CONCLUSIONS

In this thesis, a parametric model for a double circular slotted arc track mechanism with a screw jack drive for a single-slotted trailing edge flap is presented after reviewing related studies and developing a background knowledge about trailing edge flaps and mechanisms. The aim is to reduce fairing drag resulting from dropped-hinge trailing edge flap mechanism fairings. The kinematic formulation, static force analysis with force/moment equilibrium and total power equations, screw jack torque requirement of the said mechanism are derived. The parametric model is used in the design methodology chapter and these model and methodology constitute the main novelty of the thesis. A case study for a small aircraft is worked on and its motor torque requirement is determined. As a result, it is shown that the fairing depth is reduced by a considerable amount.

This thesis only presents a kinetostatic design methodology. Constructional design of the model and proper fairing design can be implemented in future works.

REFERENCES

Jie, Y. (2009). Novel swing arm mechanism design for trailing edge flaps on commercial airliner. MSc Thesis, Cranfield University.

Pires, R.M.M. (2007). Design methodology for wing trailing edge device mechanisms. PhD thesis, Cranfield University.

Zaccai, D. (2014). Design framework for trailing edge high-lift systems a knowledge based engineering application. MSc thesis, Delft University of Technology.

Flaig, A. & Hilbig, R. (1993). High-lift design for large civil aircraft. *High-lift System Aerodynamics, AGARD-CP-515* pp. 31-1-31-12.

Anderson, J. D. Jr. (2010). *Fundamentals of Aerodynamics* (5th ed). McGraw-Hill.

McCormick B. W. (1979). *Aerodynamics, Aeronautics and Flight Mechanics.* John Wiley & Sons.

Williams, J., Butler, S. F. J. &Wood M.N. (1961). *The Aerodynamics of Jet Flaps.*

Bertin, J.J. & Cummings, R.M. (2014). *Aerodynamics for Engineers* (6th ed). Pearson.

Anderson J. D. Jr. (1999). *Aircraft Performance and Design* (3rd ed). WCB/McGraw-Hill.

Lima, D.Z., Aguiar, J. B. d. & Ferreira W. (2021). Preliminary structural design of a fowler flap high-lifting device. *SAE International*. https://doi.org/10.4271/2020-36-0028

Zaccai, D., Bertels, FGA. & Vos, R. (2016). Design methodology for trailing-edge high-lift mechanisms. *CEAS Aeronautical Journal*, 7(4), 521-534. https://doi.org/10.1007/s13272-016-0202-7

Shi, Y., Song, W. & Qi, Y. (2019). A Multidisciplinary Design Framework for Mechanisms of HLDs. *American Institute of Aeronautics and Astronautics*. https://doi.org/10.2514/6.2019-3199

Guering, B. (2015). High-lift trailing edge flap system for an aircraft wing unit. US 2015/0090843 A1.

Vervliet, A.M., Raets, M., Quettier, G.T.E.M.G., Wild, J.W. & Everaert, B.A.H. (2018) Airfoil trailing edge high-lift device and actuation system therefore. EP 3 378 759 A1.

Rudolph, P.K.C. (1996). High-lift systems on commercial subsonic airliners. *NASA Contractor Report 4746*.

Söylemez, E. (2018). *Mechanisms* (5th ed) METU Press.

Hibbeler, R.C. (2009). *Engineering Mechanics: Statics* (12th ed) Prentice Hall.

Budynas, R. & Nisbett, J.K. (2006). *Shigley's mechanical engineering design* (8th ed) McGraw-Hill.

Jackson, P. (2004). *Jane's all the world's aircraft* pp. 22-23.

Houghton, E.L., Carpenter, P.W., Collicott, S.H. & Valentine, D.T. (2017). *Aerodynamics for engineering students* (7th ed). Elsevier.

NACA 63-212 AIRFOIL (n63212-il). (n.d.). http://airfoiltools.com/airfoil/details?airfoil=n63212-il

Ugural A. C. (2015). *Mechanical Design of Machine Components* (2nd ed) CRC Press.

Screw Jack Introduction. (n.d.). https://www.liftingmotion.com/screw-jack-introduction/

APPENDIX A

Three views of a typical flap of a unswept trapezoidal wing with supportive global coordinate axes (XYZ) are illustrated below, using Solidworks.

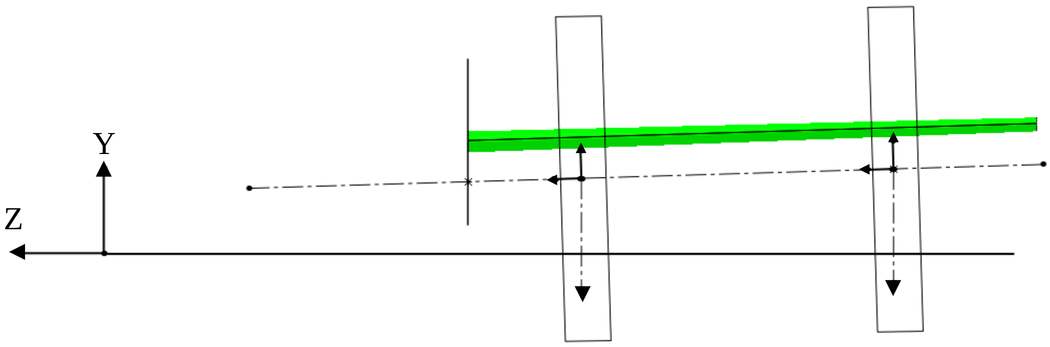

Figure 32. Front view of left (port) wing flap

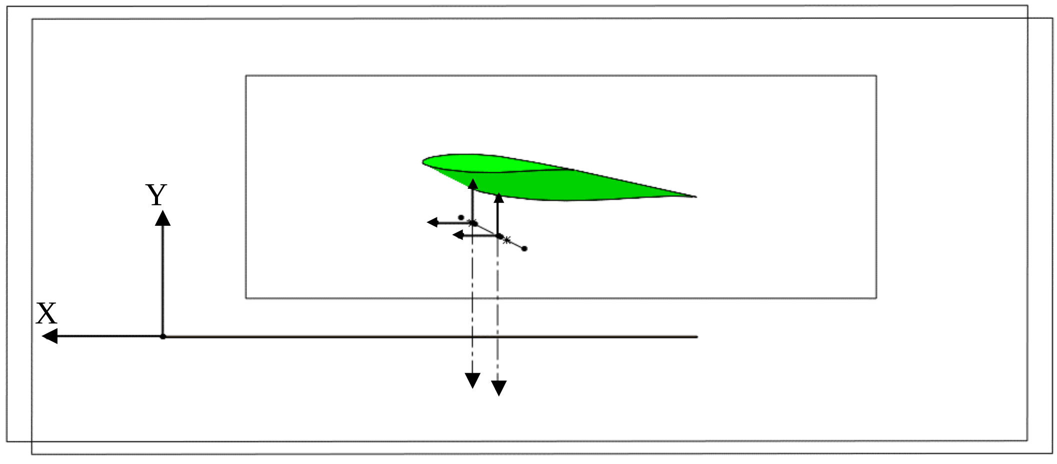

Figure 33. Side view of left flap

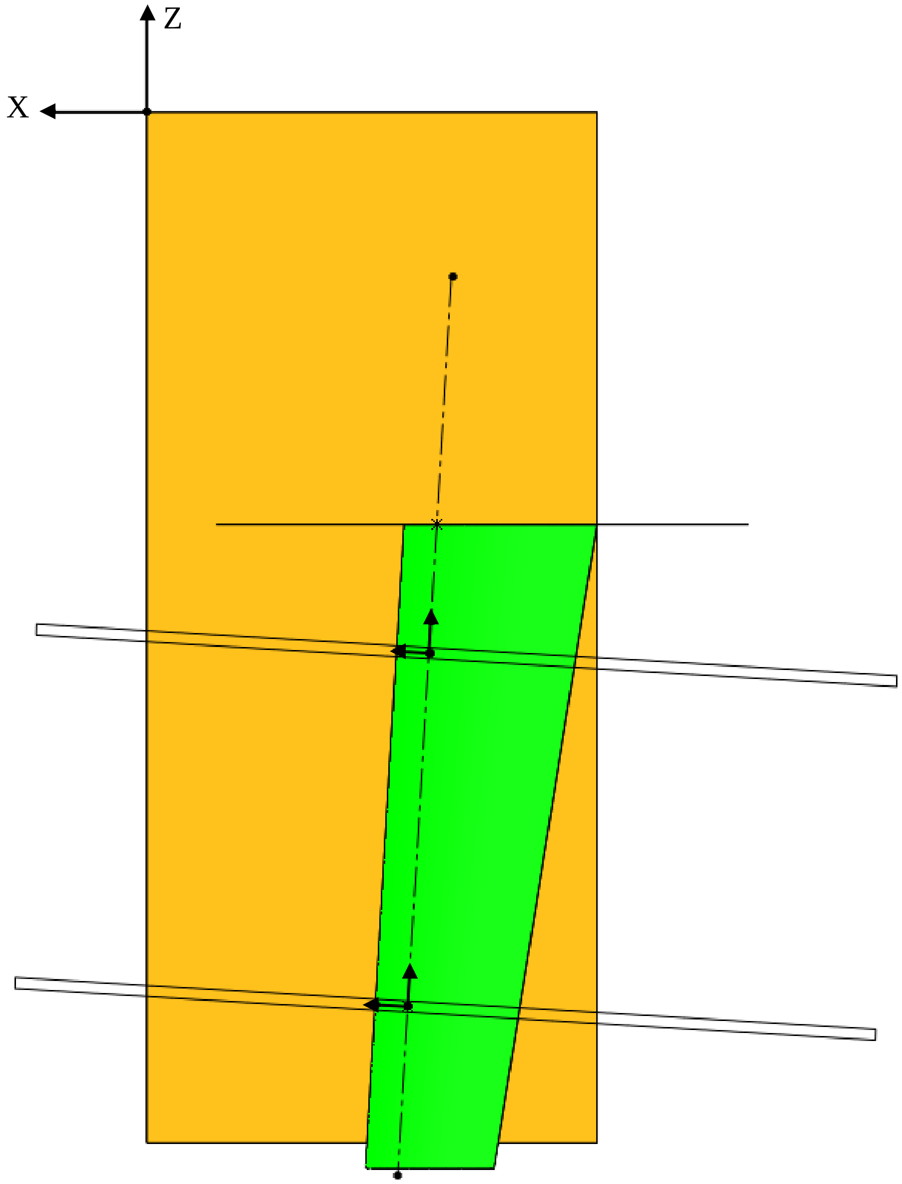

Figure 34. Top view of left flap

APPENDIX B

Determining the mechanism planes, small angle assumption with global-local coordinate axes and rotation axis are visualized via Catia, below.

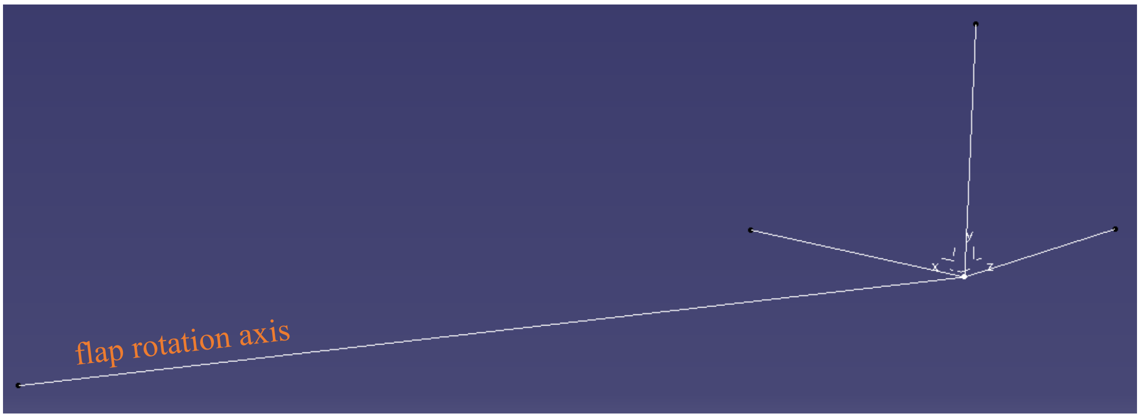

Figure 35. Rotation axis and translated global coordinate frame

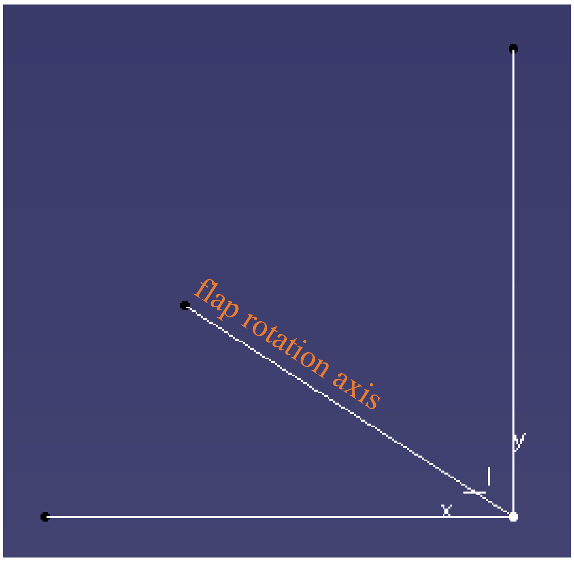

Figure 36. View normal to XY plane

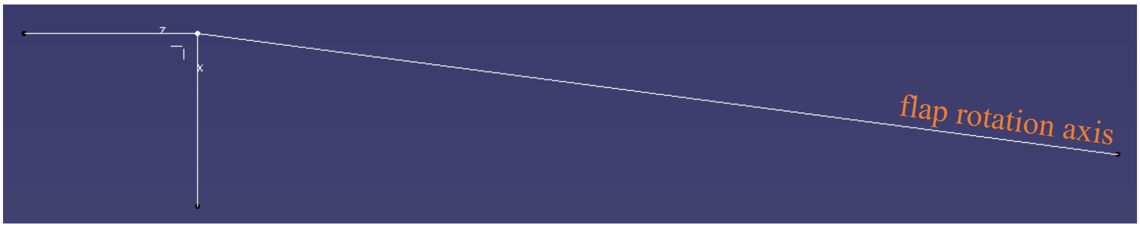

Figure 37. View normal XZ plane

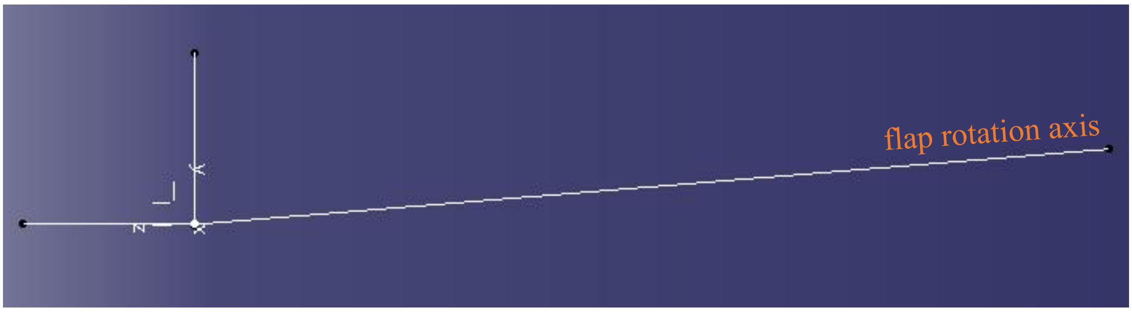

Figure 38. View normal to YZ plane

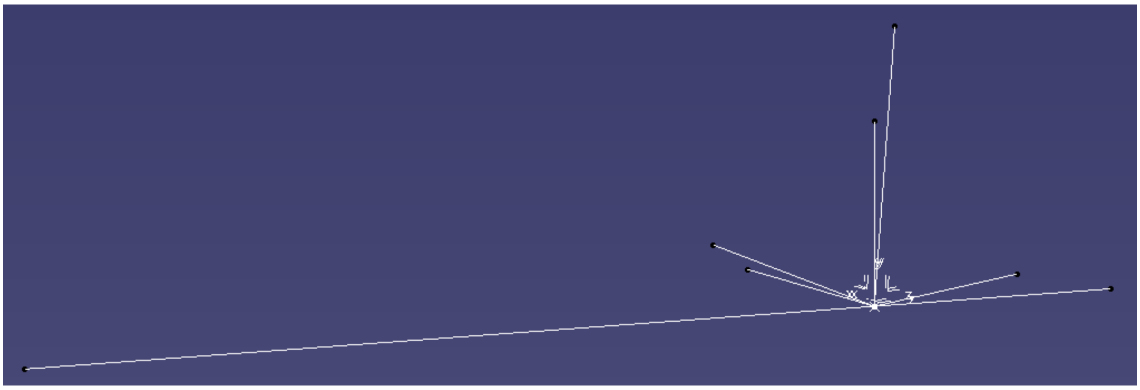

Figure 39. Local coordinate frame on global coordinate frame

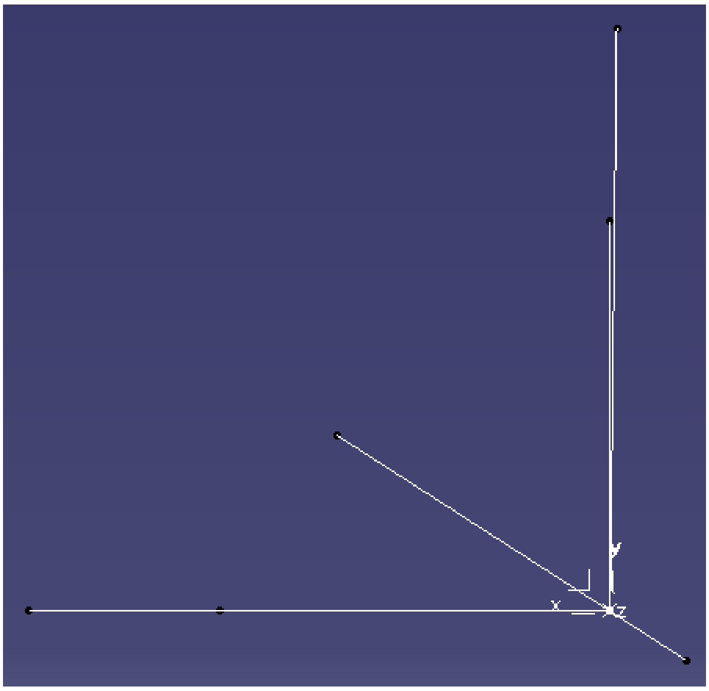

Figure 40. View normal to XY plane with local coordinate frame

Figure 41. View normal to XZ plane with local coordinate frame

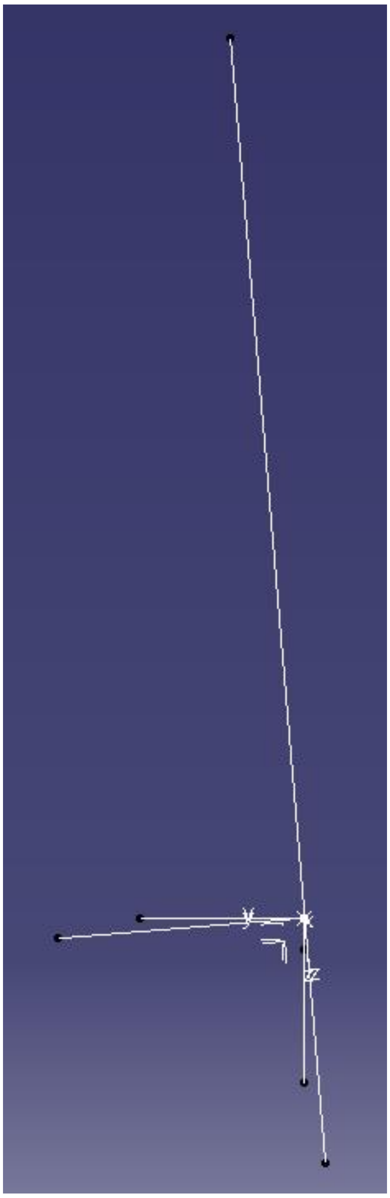

Figure 42. View normal to YZ plane with local coordinate frame

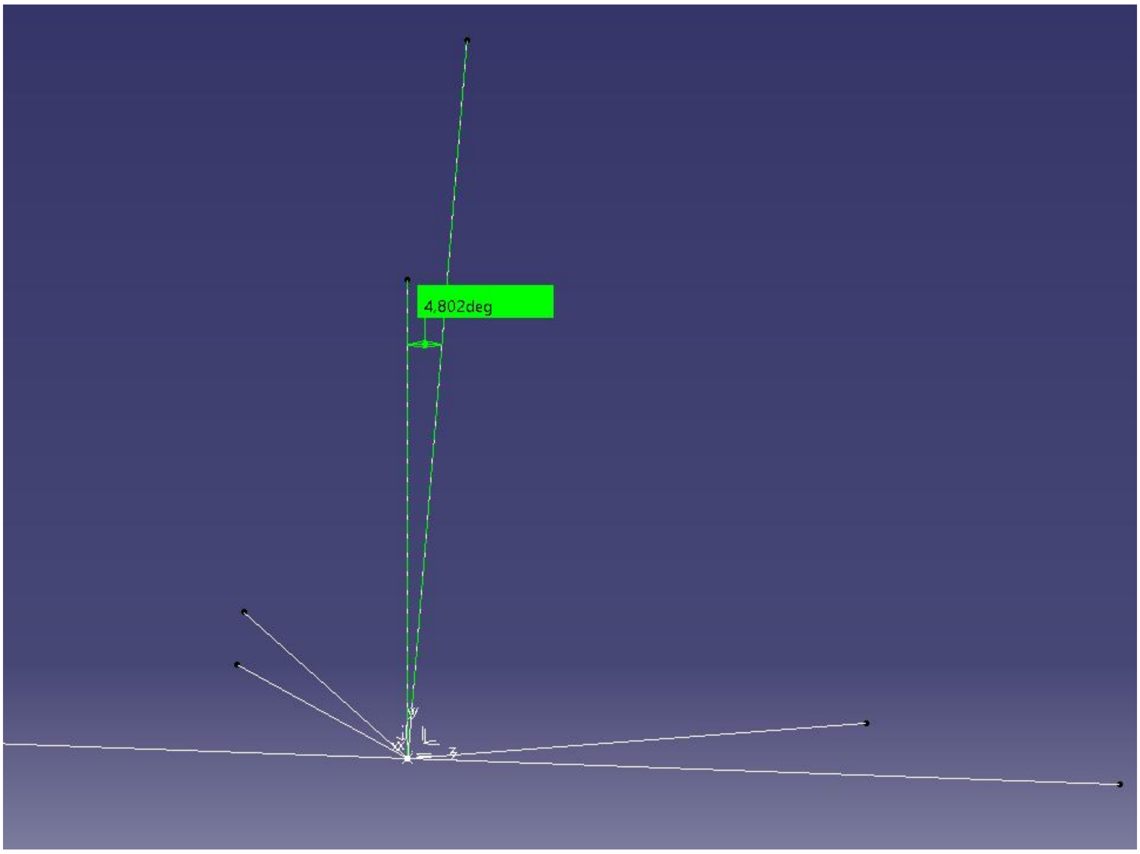

Figure 43. Small angle assumption

APPENDIX C

Since Excel worksheet cannot fit in an A4 sized paper, it is provided below in multiple pages.

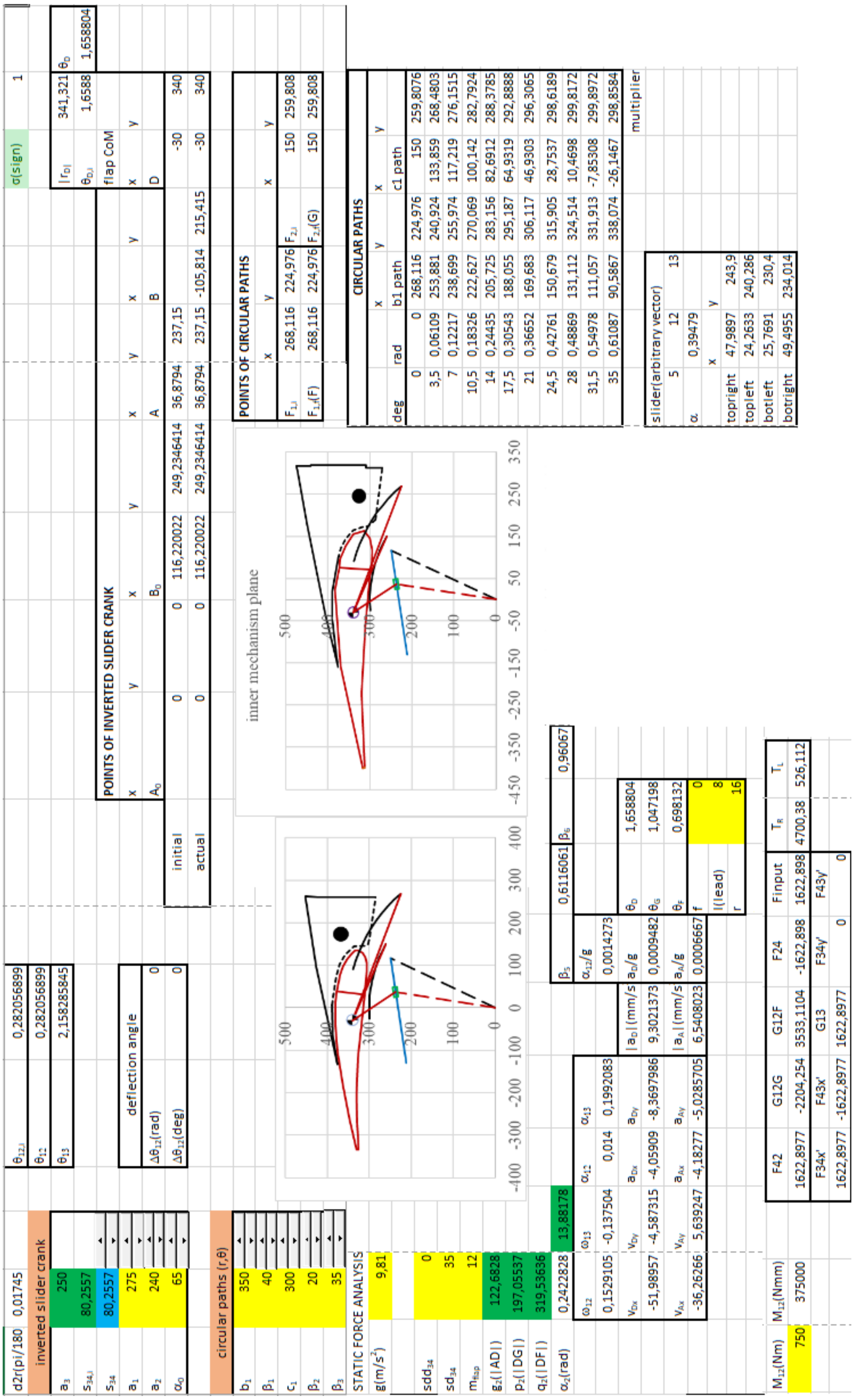

Figure 44. Variable, computed and input parameters with their spin buttons

FLAP BOUNDARY(inner)						
flap initial pos.	x	y	rad wrt horizonta	flap actual pos.	x	y
bottom part	-398	312	2,476734033		-398	312
	-223	320	2,179421895		-223	320
	-64	311	1,773750816		-64	311
	71	298	1,336901929		71	298
nose	81	296	1,30368689		81	296
	116	294	1,194990268		116	294
	146	300	1,117872167		146	300
	162,5	313,9	1,093104342		162,5	313,9
	154,3	339	1,143657779		154,3	339
	127,5	357,8	1,228480765		127,5	357,8
	95	370,5	1,31979364		95	370,5
top part	75,1	373	1,372112174		75,1	373
	21,9	382,8	1,513648589		21,9	382,8
	-158,3	370	1,975068191		-158,3	370
	-399,4	317	2,470710804		-399,4	317
outer flap spar					31,05728574	311,1538767
					38,41149856	378,1541574
inner flap spar					71	298
					75,1	373

polar coord (win(	r	θ(deg)	θ(rad)	x	y
front spar	413,2	40,8	0,712094335	312,790357	269,9933936
	439,6	44,6	0,778416846	313,0066498	308,6664821
	443,8	44,1	0,7696902	318,7044509	308,8460991
	544,3	54,1	0,944223125	319,1624738	440,9056649
	542,5	54,3	0,947713784	316,5711072	440,5553133
	570,8	56,3	0,982620369	316,7051992	474,8794129
wing top	561,3	57,1	0,996583003	304,8838188	471,27863
	483,7	68,3	1,192059879	178,8465065	449,4214249
	407,2	95,1	1,659808119	-36,19775768	405,5879218
	407,8	113	1,972222055	-159,3401542	375,3818792

flap top	r	θ(deg)	θ(rad)	x	y
	388,3	75,6	1,319468915	96,56628319	376,1008415
	389,6	87	1,518436449	20,39008855	389,0660667
	392,6	97,2	1,696460033	-49,2058275	389,5042317
	401,6	108,7	1,897172897	-128,758177	380,3996475
	405,9	111,6	1,947787445	-149,4217559	377,3962756
flap in front of n(	388,3	75,6	1,319468915	96,56628319	376,1008415
	388,6	71,9	1,254891732	120,7288606	369,3704133
	385,5	68,1	1,188569221	143,7867902	357,6808759
	376,8	64,1	1,118756051	164,5869139	338,9533711
	360	61,4	1,071632161	172,3290689	316,0738712
	350,3	60,4	1,054178868	173,0278359	304,5840738
	343,4	56,7	0,989601686	188,5344357	287,0162479
wing below spar	343,4	56,7	0,989601686	188,5344357	287,0162479
	449,4	35,9	0,626573201	315	270
torque tube					
	408	53,3	0,930260491	243,83106	327,1244629

FLAP BOUNDARY(outer)					
polar coord	r	θ(deg)	θ(rad)	x	y
spar front	385,7	47,6	0,830776724	260,0784309	284,8222249
	409	50,5	0,881391272	260,1559921	315,5944546
	497,8	58,5	1,021017612	260,0997855	424,4442738
	522,2	60,1	1,04894288	260,3102977	452,6934823
wing top	522,2	60,1	1,04894288	260,3102977	452,6934823
	436,7	77,4	1,350884841	95,26315352	426,1828499
	399,6	109,6	1,91288086	-134,0464473	376,4461581
flap top	399,6	109,6	1,91288086	-134,0464473	376,4461581
	391,9	99,4	1,734857276	-64,0074446	386,6376301
	388,5	89,2	1,556833693	5,424307062	388,4621306
flap boundary ne	388,5	89,2	1,556833693	5,424307062	388,4621306
	385,2	79,2	1,382300768	72,17928238	378,377049
	383,6	74,8	1,30550628	100,5757689	370,1803273
	378,5	70,8	1,23569311	124,4760258	357,4464561
	365,2	66,9	1,16762527	143,281515	335,9188108
	340,9	64,7	1,129228026	145,6862956	308,2017412
	337,1	63,7	1,111774734	149,3592984	302,2055757
wing below spar	337,1	63,7	1,111774734	149,3592984	302,2055757
	341,5	61,5	1,07337749	162,9497166	300,116044
	385,7	47,6	0,830776724	260,0784309	284,8222249
flap	466,4	135,8	2,370157124	-334,3671074	325,157804
	429,3	130,1	2,270673357	-276,5222743	328,3807574
	390	122,2	2,132792346	-207,8217477	330,0153348
	347,9	110	1,919862177	-118,9888079	326,9190628
	312,7	84,3	1,471312559	31,05728574	311,1538767
	315,5	77,5	1,35263017	68,2866982	308,0213902
	318,6	74,1	1,293288976	87,28340708	306,4107812
	323,6	71,3	1,244419757	103,7503638	306,5172459
	331,4	69,1	1,206022513	118,222973	309,5953628
	340,8	67,9	1,185078562	128,2172289	315,7609574
	353,4	67,7	1,181587904	134,0998068	326,9691145
	359	68	1,186823891	134,483767	332,8590038
	363,9	69,5	1,21300383	127,440466	340,8550097
	370,2	72,1	1,258382391	113,7834199	352,2802483
	374,4	75,2	1,312487597	95,63889177	361,9786767
	376,7	78	1,361356817	78,32033393	368,4682012
	380,1	84,2	1,46956723	38,41149856	378,1541574
	380,5	87,9	1,534144413	13,94293116	380,2444538
	383,5	96,2	1,67900674	-41,41775291	381,2568947
	388,9	105,2	1,836086373	-101,9653716	375,2949147
	406,5	116,6	2,035053908	-182,0140692	363,4736973
	436,9	127,4	2,223549467	-265,3625044	347,0797477
	470	135,4	2,363175807	-334,6522416	330,0119349
	466,4	135,8	2,370157124	-334,3671074	325,157804
	x	y	θ(rad)		
torque tube	172,5	367,7	1,132146263		

Figure 45. Boundaries of a small aircraft

10	s_{34}	s_{34}	θ_{12}	θ_{13}	ω_{12}	ω_{13}	α_{12}	α_{13}	v_{Ax}	v_{Ay}	a_{Ax}	a_{Ay}	v_{Dx}	v_{Dy}	a_{Dx}	a_{Dy}
0	80,255741	80,25574	0,28206	2,1582858	0,1529105	-0,137504	0,0140016	0,199208	-36,263	5,63925	-4,182771046	-5,02857	-51,9896	-4,58731	-4,05909	-8,3698
1	90,255741	90,25574	0,32526	2,1261113	0,1497794	-0,09082	0,0084398	0,133638	-35,726	3,98449	-2,609875832	-5,12643	-50,6834	-6,68866	-1,85411	-7,96823
2	100,25574	100,2557	0,36776	2,1050216	0,1478775	-0,058657	0,0051316	0,094616	-35,407	2,43174	-1,588290872	-5,15154	-49,7141	-8,72382	-0,43511	-7,65432
3	110,25574	110,2557	0,40983	2,0917503	0,1467383	-0,03542	0,0029825	0,069789	-35,205	0,93308	-0,85246215	-5,14693	-48,9233	-10,7239	0,57923	-7,39689
4	120,25574	120,2557	0,45166	2,0842311	0,146112	-0,018002	0,0014832	0,053187	-35,063	-0,53747	-0,277394874	-5,12855	-48,2254	-12,7057	1,36691	-7,17529
5	130,25574	130,2557	0,49336	2,0810877	0,1458542	-0,004549	0,0003714	0,041648	-34,948	-1,99523	0,202016543	-5,10241	-47,5697	-14,6792	2,01989	-6,97563
6	140,25574	140,2557	0,53503	2,0813662	0,145877	0,0061055	-0,000499	0,033376	-34,84	-3,4499	0,622405804	-5,07057	-46,9242	-16,6507	2,58942	-6,78823
7	150,25574	150,2557	0,57674	2,084384	0,1461246	0,0147304	-0,001214	0,027298	-34,725	-4,90797	1,005706014	-5,03337	-46,2676	-18,6244	3,10593	-6,60608
8	160,25574	160,2557	0,61855	2,0896405	0,1465612	0,0218482	-0,001828	0,022738	-34,592	-6,37402	1,365755658	-4,99038	-45,5845	-20,6033	3,58836	-6,42387
9	170,25574	170,2557	0,66051	2,0967605	0,1471633	0,0278264	-0,002377	0,019262	-34,435	-7,85149	1,711702148	-4,9408	-44,8637	-22,5896	4,04907	-6,23739
10	180,25574	180,2557	0,70266	2,1054582	0,1479157	0,0329298	-0,002884	0,016575	-34,248	-9,3431	2,049860844	-4,88365	-44,0963	-24,5851	4,49644	-6,0431
11	190,25574	190,2557	0,74504	2,1155129	0,1488093	0,0373537	-0,003368	0,014477	-34,026	-10,8511	2,384781526	-4,81779	-43,2748	-26,5912	4,93637	-5,8379
12	200,25574	200,2557	0,7877	2,1267525	0,1498391	0,0412451	-0,00384	0,012828	-33,764	-12,3774	2,719886691	-4,742	-42,3927	-28,6092	5,37317	-5,61892
13	210,25574	210,2557	0,83068	2,1390416	0,1510034	0,0447169	-0,004311	0,011526	-33,459	-13,9239	3,057868357	-4,65492	-41,4441	-30,6403	5,81008	-5,38337
14	220,25574	220,2557	0,874	2,1522735	0,1523035	0,0478573	-0,004791	0,010498	-33,107	-15,4923	3,400943582	-4,55505	-40,4231	-32,6856	6,24967	-5,12843
15	230,25574	224,5945	0,89292	2,1582858	0,1529105	0,049135	-0,005003	0,010123	-32,939	-16,18	3,551871308	-4,50733	-39,9562	-33,5777	6,44176	-5,01105
16	240,25574	224,5945	0,89292	2,1582858	0,1529105	0,049135	-0,005003	0,010123	-32,939	-16,18	3,551871308	-4,50733	-39,9562	-33,5777	6,44176	-5,01105
17	250,25574	224,5945	0,89292	2,1582858	0,1529105	0,049135	-0,005003	0,010123	-32,939	-16,18	3,551871308	-4,50733	-39,9562	-33,5777	6,44176	-5,01105
18	260,25574	224,5945	0,89292	2,1582858	0,1529105	0,049135	-0,005003	0,010123	-32,939	-16,18	3,551871308	-4,50733	-39,9562	-33,5777	6,44176	-5,01105
19	270,25574	224,5945	0,89292	2,1582858	0,1529105	0,049135	-0,005003	0,010123	-32,939	-16,18	3,551871308	-4,50733	-39,9562	-33,5777	6,44176	-5,01105
20	280,25574	224,5945	0,89292	2,1582858	0,1529105	0,049135	-0,005003	0,010123	-32,939	-16,18	3,551871308	-4,50733	-39,9562	-33,5777	6,44176	-5,01105

A_x	A_y	D_x	D_y	θ_D	θ_G	θ_F	F_{42}	G_{12G}	G_{12F}	F_{24}	F_{input}	T_R	T_L	$\lvert a_A \rvert/g*100$	$\lvert a_D \rvert/g*100$	$mgr_D\cos\theta_D$
36,8794	237,15	-30	340	1,6588	1,0472	0,69813	1622,9	-2204,25	3533,11	-1622,9	1622,9	4700,38	526,112	0,066674845	0,09482301	-3531,6
26,6024	238,521	-44,6567	338,387	1,70201	1,0904	0,74134	1582,28	-2443,02	3660,8	-1582,28	1582,28			0,058639587	0,083395502	-5256,99222
16,4443	239,436	-58,9935	336,184	1,74451	1,1329	0,78384	1555,06	-2636,13	3763,6	-1555,06	1555,06			0,054952384	0,078151669	-6944,72062
6,35881	239,916	-73,0816	333,405	1,78658	1,17497	0,82591	1536,13	-2799,4	3850,16	-1536,13	1536,13			0,053180951	0,075632389	-8603,16378
-3,67845	239,972	-86,9585	330,058	1,82841	1,2168	0,86773	1522,75	-2942,1	3925,57	-1522,75	1522,75			0,052355199	0,07445803	-10236,7519
-13,6796	239,61	-100,643	326,146	1,87011	1,2585	0,90944	1513,35	-3070,07	3993,01	-1513,35	1513,35			0,052053089	0,074028377	-11847,6863
-23,6494	238,832	-114,142	321,67	1,91178	1,30017	0,95111	1506,96	-3187,22	4054,64	-1506,96	1506,96			0,052075691	0,074060521	-13436,8103
-33,5875	237,638	-127,456	316,631	1,95349	1,34188	0,99282	1502,98	-3296,31	4111,95	-1502,98	1502,98			0,052322696	0,074411804	-15004,0852
-43,4905	236,027	-140,578	311,027	1,9953	1,38369	1,03462	1501	-3399,34	4166,06	-1501	1501			0,052740981	0,075006676	-16548,8656
-53,3523	233,995	-153,5	304,857	2,03725	1,42565	1,07658	1500,77	-3497,82	4217,79	-1500,77	1500,77			0,053301784	0,075804235	-18070,0652
-63,165	231,539	-166,21	298,118	2,0794	1,4678	1,11873	1502,12	-3592,95	4267,81	-1502,12	1502,12			0,053989911	0,076782869	-19566,2601
-72,9193	228,654	-178,693	290,807	2,12179	1,51018	1,16112	1504,95	-3685,69	4316,64	-1504,95	1504,95			0,05479833	0,077932578	-21035,7531
-82,6046	225,336	-190,933	282,922	2,16445	1,55284	1,20378	1509,19	-3776,82	4364,72	-1509,19	1509,19			0,055725368	0,079250984	-22476,6142
-92,209	221,58	-202,911	274,458	2,20742	1,59582	1,24675	1514,84	-3867,02	4412,42	-1514,84	1514,84			0,056773222	0,080741211	-23886,7039
-101,72	217,378	-214,608	265,412	2,25075	1,63915	1,29008	1521,89	-3956,91	4460,09	-1521,89	1521,89			0,057947185	0,082410788	-25263,6863
-105,814	215,415	-219,591	261,304	2,26967	1,65806	1,309	1525,39	-3995,95	4480,84	-1525,39	1525,39			0,058497706	0,083193722	-25850,1995
-105,814	215,415	-219,591	261,304	2,26967	1,65806	1,309	1525,39	-3995,95	4480,84	-1525,39	1525,39			0,058497706	0,083193722	-25850,1995
-105,814	215,415	-219,591	261,304	2,26967	1,65806	1,309	1525,39	-3995,95	4480,84	-1525,39	1525,39			0,058497706	0,083193722	-25850,1995
-105,814	215,415	-219,591	261,304	2,26967	1,65806	1,309	1525,39	-3995,95	4480,84	-1525,39	1525,39			0,058497706	0,083193722	-25850,1995
-105,814	215,415	-219,591	261,304	2,26967	1,65806	1,309	1525,39	-3995,95	4480,84	-1525,39	1525,39			0,058497706	0,083193722	-25850,1995
-105,814	215,415	-219,591	261,304	2,26967	1,65806	1,309	1525,39	-3995,95	4480,84	-1525,39	1525,39			0,058497706	0,083193722	-25850,1995

Figure 46. Cells used in position, velocity, acceleration level analyses and force calculations

CASE STUDY implementation									A_i	x	y	A_f	x	y
										-120	207,8461		-217,51	101,428
t	152,425		A_i		A_f				B		D			
$s_{34,i}$	80,2557		x	y	x	y			x	y	x	y		
			36,8794	237,149552	-105,8136	215,4147			-108,3745	249,23464	-30	340		
Δs	144,339				b_1		c_1				$\|r_D\|$	341,321		
μ_{min}	1,26536	72,5	deg	rad	x	y	x	y			θ_D	1,658804		
$\theta_{13,i}$	2,15829		0	0	350	0	300	0			$D_{xactual}$	$D_{yactual}$		
			5	0,08726646	348,66814	30,50451	298,858	26,146723			-30	340		
			10	0,17453293	344,68271	60,77686	295,442	52,094453	185	3,22885912	-348,6681	-30,50451	-298,858	-26,146723
			15	0,26179939	338,07404	90,58667	289,778	77,645714	190	3,31612558	-344,6827	-60,77686	-295,442	-52,094453
			20	0,34906585	328,89242	119,7071	281,908	102,60604	195	3,40339204	-338,074	-90,58667	-289,778	-77,645714
			25	0,43633231	317,20773	147,9164	271,892	126,78548	200	3,4906585	-328,8924	-119,7071	-281,908	-102,60604
			30	0,52359878	303,10889	175	259,808	150	205	3,57792497	-317,2077	-147,9164	-271,892	-126,78548
			35	0,61086524	286,70322	200,7518	245,746	172,07293	210	3,66519143	-303,1089	-175	-259,808	-150
			40	0,6981317	268,11556	224,9757	229,813	192,83628	215	3,75245789	-286,7032	-200,7518	-245,746	-172,07293
			45	0,78539816	247,48737	247,4874	212,132	212,13203	220	3,83972435	-268,1156	-224,9757	-229,813	-192,83628
			50	0,87266463	224,97566	268,1156	192,836	229,81333	225	3,92699082	-247,4874	-247,4874	-212,132	-212,13203
			55	0,95993109	200,75175	286,7032	172,073	245,74561	230	4,01425728	-224,9757	-268,1156	-192,836	-229,81333
			60	1,04719755	175	303,1089	150	259,80762	235	4,10152374	-200,7518	-286,7032	-172,073	-245,74561
			65	1,13446401	147,91639	317,2077	126,785	271,89234	240	4,1887902	-175	-303,1089	-150	-259,80762
			70	1,22173048	119,70705	328,8924	102,606	281,90779	245	4,27605667	-147,9164	-317,2077	-126,785	-271,89234
			75	1,30899694	90,586666	338,074	77,6457	289,77775	250	4,36332313	-119,7071	-328,8924	-102,606	-281,90779
			80	1,3962634	60,776862	344,6827	52,0945	295,44233	255	4,45058959	-90,58667	-338,074	-77,6457	-289,77775
			85	1,48352986	30,50451	348,6681	26,1467	298,85841	260	4,53785606	-60,77686	-344,6827	-52,0945	-295,44233
			90	1,57079633	2,144E-14	350	1,8E-14	300	265	4,62512252	-30,50451	-348,6681	-26,1467	-298,85841
			95	1,65806279	-30,50451	348,6681	-26,1467	298,85841	270	4,71238898	-6,43E-14	-350	-5,5E-14	-300
			100	1,74532925	-60,77686	344,6827	-52,0945	295,44233	275	4,79965544	30,50451	-348,6681	26,1467	-298,85841
			105	1,83259571	-90,58667	338,074	-77,6457	289,77775	280	4,88692191	60,776862	-344,6827	52,0945	-295,44233
			110	1,91986218	-119,7071	328,8924	-102,606	281,90779	285	4,97418837	90,586666	-338,074	77,6457	-289,77775
			115	2,00712864	-147,9164	317,2077	-126,785	271,89234	290	5,06145483	119,70705	-328,8924	102,606	-281,90779
			120	2,0943951	-175	303,1089	-150	259,80762	295	5,14872129	147,91639	-317,2077	126,785	-271,89234
			125	2,18166156	-200,7518	286,7032	-172,073	245,74561	300	5,23598776	175	-303,1089	150	-259,80762
			130	2,26892803	-224,9757	268,1156	-192,836	229,81333	305	5,32325422	200,75175	-286,7032	172,073	-245,74561
			135	2,35619449	-247,4874	247,4874	-212,132	212,13203	310	5,41052068	224,97566	-268,1156	192,836	-229,81333
			140	2,44346095	-268,1156	224,9757	-229,813	192,83628	315	5,49778714	247,48737	-247,4874	212,132	-212,13203
			145	2,53072742	-286,7032	200,7518	-245,746	172,07293	320	5,58505361	268,11556	-224,9757	229,813	-192,83628
			150	2,61799388	-303,1089	175	-259,808	150	325	5,67232007	286,70322	-200,7518	245,746	-172,07293
			155	2,70526034	-317,2077	147,9164	-271,892	126,78548	330	5,75958653	303,10889	-175	259,808	-150
			160	2,7925268	-328,8924	119,7071	-281,908	102,60604	335	5,84685299	317,20773	-147,9164	271,892	-126,78548
			165	2,87979327	-338,074	90,58667	-289,778	77,645714	340	5,93411946	328,89242	-119,7071	281,908	-102,60604
			170	2,96705973	-344,6827	60,77686	-295,442	52,094453	345	6,02138592	338,07404	-90,58667	289,778	-77,645714
			175	3,05432619	-348,6681	30,50451	-298,858	26,146723	350	6,10865238	344,68271	-60,77686	295,442	-52,094453
			180	3,14159265	-350	4,29E-14	-300	3,675E-14	355	6,19591884	348,66814	-30,50451	298,858	-26,146723
									360	6,28318531	350	-8,58E-14	300	-7,351E-14

Figure 47. Cells used in case study drawings

	Landing scenario											
			2 jack screws									
35	M_{12}max	650	325000									
0	M_{12}min	220	110000									
		ΔT	215000									
	M_{12}	F_{input}	T_R	T_L	T_R/1000	T_L/1000	M_{12}/1000	G_{12G}	G_{12F}	$M_{12}+\|mgr_D\cos\theta_D\|$		$[\|mgr_D\cos\theta_D\|/(M_{12}+\|mgr_D\cos\theta_D\|)]*100$
	110000	465,147	1347,2	150,792	1,3472	0,150792	110	-443,677	889,872	113532		3,11068
	124896	511,983	1482,85	165,975	1,48285	0,165975	124,896	-618,774	1076,94	130153		4,0391
	139791	561,285	1625,64	181,958	1,62564	0,181958	139,791	-795,71	1265,17	146736		4,73281
	154687	612,458	1773,85	198,547	1,77385	0,198547	154,687	-975,831	1455,27	163290		5,26865
	169582	665,208	1926,63	215,647	1,92663	0,215647	169,582	-1159,92	1647,68	179819		5,69282
	184478	719,394	2083,57	233,214	2,08357	0,233214	184,478	-1348,49	1842,66	196325		6,03472
	199373	774,966	2244,53	251,229	2,24453	0,251229	199,373	-1541,95	2040,43	212810		6,314
	214269	831,927	2409,5	269,695	2,4095	0,269695	214,269	-1740,61	2241,17	229273		6,54421
	229164	890,318	2578,62	288,624	2,57862	0,288624	229,164	-1944,78	2445,05	245713		6,73504
	244060	950,21	2752,08	308,04	2,75208	0,30804	244,06	-2154,75	2652,23	262130		6,89356
	258955	1011,7	2930,16	327,972	2,93016	0,327972	258,955	-2370,81	2862,87	278521		7,02505
	273851	1074,89	3113,19	348,459	3,11319	0,348459	273,851	-2593,28	3077,15	294886		7,13351
	288746	1139,93	3301,57	369,544	3,30157	0,369544	288,746	-2822,5	3295,26	311223		7,22203
	303642	1206,97	3495,73	391,276	3,49573	0,391276	303,642	-3058,84	3517,42	327528		7,29302
	318537	1276,19	3696,21	413,715	3,69621	0,413715	318,537	-3302,7	3743,83	343801		7,34835
	325000	1306,95	3785,29	423,687	3,78529	0,423687	325	-3410,95	3843,46	350850		7,36787
	325000	1306,95	3785,29	423,687	3,78529	0,423687	325	-3410,95	3843,46	350850		7,36787
	325000	1306,95	3785,29	423,687	3,78529	0,423687	325	-3410,95	3843,46	350850		7,36787
	325000	1306,95	3785,29	423,687	3,78529	0,423687	325	-3410,95	3843,46	350850		7,36787
	325000	1306,95	3785,29	423,687	3,78529	0,423687	325	-3410,95	3843,46	350850		7,36787
	325000	1306,95	3785,29	423,687	3,78529	0,423687	325	-3410,95	3843,46	350850		7,36787
			4700,38	526,112			max	-3410,95	3843,46			
			|T,max|	4700,38			min	-443,677	889,872			

Figure 48. Cells used in landing scenario calculations